

**Document: PO-TN-IMK-GS-0003**

**ESA-Contract No. 11717/95/NL/CN**

**ESA-Contract No. 12078/96/NL/GS**

**Technical Note**

# **Level 0 to 1b Data Processing of the MIPAS-B2 balloon borne Fourier Transform Spectrometer**

**Revision 1.2 of 17.05.2000**

**by O. Trieschmann**  
**with inputs from F. Friedl-Vallon, A. Kleinert, A. Lengel, G. Wetzel**  
**approved by H. Oelhaf**

**Forschungszentrum Karlsruhe**  
**Institut für Meteorologie and Klimaforschung**  
**P.O. Box 3640**  
**D-76021 Karlsruhe**

## **History:**

**Draft Version – February 1998**

**Revision 1 – 03.04.2000**

Added:

- Updated algorithm description
- Description of ILS determination
- Description of the level 1b parametrization
- ILS-parametrisation

**Revision 1.1 – 17.04.2000**

Comments by H. Nett are considered in subsections 6.5.1, 6.6, 7.3.1, 7.5.1, 7.5.3 and 8.2.

**Revision 1.2 – 17.05.2000**

Updated subsection 7.5.3.

# 1. Table of contents

<b>1. Table of contents</b> .....	<b>3</b>
<b>2. Introduction</b> .....	<b>5</b>
<b>3. Typical measuring scenarios</b> .....	<b>7</b>
<b>4. Definition of the data levels</b> .....	<b>9</b>
<b>5. Description of the processing chain</b> .....	<b>10</b>
<b>6. Overview of the processing algorithms of MIPAS-B2</b> .....	<b>13</b>
6.1. Differences between MIPAS-B2 and MIPAS/ENVISAT data processing .....	13
6.2. Phase correction of interferograms .....	14
6.2.1. <i>Methods for phase determination and correction for MIPAS-B2</i> .....	15
6.2.2. <i>Results</i> .....	20
6.3. Spectral and Radiometric Calibration .....	21
6.4. Localisation .....	22
6.5. ILS determination .....	22
6.5.1. <i>ILS parameterization</i> .....	25
<b>7. The parameterization of the individual processes</b> .....	<b>27</b>
7.1. Interferogram processing independent of the source .....	27
7.1.1. <i>Interferogram check</i> .....	27
7.1.2. <i>Interferogram non-linearity correction</i> .....	27
7.2. Blackbody spectra .....	28
7.2.1. <i>Phase determination of blackbody interferograms</i> .....	28
7.2.2. <i>Interferogram phase correction</i> .....	29
7.2.3. <i>Generation of blackbody spectra</i> .....	29
7.2.4. <i>Co-addition of blackbody spectra</i> .....	30
7.2.5. <i>Noise reduction in blackbody spectra (only channel 3)</i> .....	30
7.3. Deep-space spectra .....	31
7.3.1. <i>Co-addition of deep-space interferograms</i> .....	31
7.3.2. <i>Phase determination of deep-space spectra</i> .....	32
7.3.3. <i>Phase correction of deep-space interferograms</i> .....	32
7.3.4. <i>Generation of deep-space spectra</i> .....	33
7.3.5. <i>Shaving of deep-space spectra</i> .....	33
7.4. Limb sequence spectra .....	33
7.4.1. <i>Phase determination of limb sequence spectra</i> .....	33
7.4.2. <i>Phase correction of limb sequence interferograms</i> .....	33
7.4.3. <i>Generation of limb sequence spectra</i> .....	34
7.5. Calibration .....	34
7.5.1. <i>Radiometric calibration of limb spectra</i> .....	34
7.5.2. <i>Interpolation on the ENVISAT spectral grid and spectral calibration</i> .....	35
7.5.3. <i>Calculation of variance of single consecutive spectra</i> .....	36
<b>8. Algorithms - Reference</b> .....	<b>37</b>

8.1.	Apodisation functions .....	38
8.2.	Co-addition of interferograms .....	41
8.3.	Co-addition of spectra .....	46
8.4.	Conditioning of data sets for FFT .....	49
8.5.	Convolution of data sets using FFT .....	51
8.6.	Fitting procedure with weighting coefficients .....	52
8.7.	Generation of spectra .....	53
8.8.	Generation of the variance of single consecutive spectra .....	56
8.9.	Interferogram correction and mathematical filtering .....	59
8.10.	Kernel generation .....	61
8.11.	Phase determination .....	63
8.11.1.	<i>'Classical' phase determination</i> .....	64
8.11.2.	<i>Differential Phase determination</i> .....	67
8.11.3.	<i>Statistical phase determination</i> .....	71
8.12.	Radiometric calibration of the spectra .....	77
8.13.	'Shaving' - Removal of residual atmospheric lines in deep space spectra .....	80
<b>9.</b>	<b>References .....</b>	<b>85</b>
<b>10.</b>	<b>Appendix .....</b>	<b>88</b>
10.1.	Abbreviation and Notation .....	88
10.2.	List of wavenumbers of critical radiometric calibration .....	89
10.2.1.	<i>Channel 1</i> .....	89
10.2.2.	<i>Channel 2</i> .....	90
10.2.3.	<i>Channel 3</i> .....	91
10.3.	Data exchange for MIPAS-B balloon data between IMK and IROE/Univ. of Bologna .....	92
10.3.1.	<i>Purpose</i> .....	92
10.3.2.	<i>Abbreviations</i> .....	92
10.3.3.	<i>Definitions and general information</i> .....	92
10.3.4.	<i>File formats</i> .....	92
10.3.4.1.	<i>Channel descriptive data sets (ESA-Contract No. 11717/95/NL/CN and ESA-Contract No. 12078/96/NL/GS)</i> .....	93
10.3.4.2.	<i>Spectral data sets (ESA-Contract No. 11717/95/NL/CN)</i> .....	94
10.3.4.3.	<i>Spectral data sets (ESA-Contract No. 12078/96/NL/GS)</i> .....	95
10.3.4.4.	<i>Pressure-temperature initial guess profile (ESA-Contract No. 11717/95/NL/CN and ESA-Contract No. 12078/96/NL/GS)</i> .....	96
10.4.	HDF data format description of delivered data .....	97
10.5.	ILS calculation from Bessel coefficients .....	99

## 2. Introduction

MIPAS (Michelson Interferometer for Passive Atmospheric Sounding) is a limb viewing interferometer measuring emission spectra of key trace species relevant to ozone chemistry in the mid-infrared spectral region between 4.15  $\mu\text{m}$  and 14.6  $\mu\text{m}$ . A satellite instrument of the MIPAS family will be operated on the ESA/ENVISAT platform and is described in detail in various papers (e.g. [Ende1993]). MIPAS-B2 [Frie1999-1] may be conceived as a precursor of MIPAS-ENVISAT. The essence of the instrument is a high resolution Fourier transform spectrometer (FTS). In Fourier transform spectroscopy highly sophisticated data analysis methods are required to derive trace gas distributions from raw data obtained by the FTS. The raw data, so-called interferograms (IFG), are to be transformed into radiometrically calibrated atmospheric spectra which are subsequently used for the trace gas retrieval.

For evaluating and validating the data processing tools similar data to the expected ones from the satellite are very valuable. The "Institut für Meteorologie und Klimaforschung" (IMK) agreed with ESA in contract 12078/96/NL/GS and in WP6000 of contract 11717/95/NL/CN to deliver the desired data products. Balloon borne measurements performed by the FTS instrument MIPAS-B2 have been used for this task. The detector optics of MIPAS-B2 has been matched to that of MIPAS-ENVISAT in terms of channel separation and spectral coverage for this purpose.

MIPAS-B2 level 1B and related instrumental data serve as input to the "Optimised Retrieval Module" (ORM) that was developed in the framework of ESA-supported studies at IROE. The use of real atmospheric spectra is supposed to be a more realistic test of the ORM and is thought to be an important step in preparing the on-line processors for MIPAS-ENVISAT.

This document describes in detail the processing steps of the MIPAS-B2 data from the raw IFGs (level 0) to the calibrated spectra (level 1b), including all intermediate products. The parameterisation of the processes as used within the level-1b data processing for the 6<sup>h</sup> flight of MIPAS-B2 on May 7/8, 1998 is given. A separate technical note related to instrument characterisation of MIPAS-B2 is available [Frie1999-2]. It is assumed that the reader is familiar with the basic principles of the Fourier transform spectroscopy, the MIPAS experiments and the issues associated with the generation of calibrated spectra from interferograms.

Chapters 3 and 4 review the measurement scenario and the data definition. In chapters 5 and 6 the overall processing chain will be discussed especially in case of differences to that of the MIPAS-Satellite Instrument. The processing will be described in physical terms to give a deeper insight into the phase correction and calibration method regarding the constraints by the optical design of the MIPAS-B instrument and the measurement scenario. In chapter 7 the algorithms together with their parameterisation will be described related to the processing of the 6<sup>th</sup> flight of MIPAS-B2. The individual processes which are used for data processing and which

are referenced in chapter 7 will be discussed in Chapter 8 in more detail, as the basis for implementing of the algorithms. The ILS determination will be described in chapter 6.5. The data products and their formats which are delivered according to the contracts are specified in the document "Data exchange for MIPAS-B balloon data between IMK and IROE/Univ. of Bologna", which is added in Appendix 0

### 3. Typical measuring scenarios

The processing of the data is linked to the measuring scenario and vice versa. Therefore, the typical constraints on the scenario for the flight of the MIPAS-B2 experiment will be outlined within this chapter.

The measuring scenario is matched to atmospheric conditions in the atmosphere at the time of the flight and the predicted duration of the float. There are some basic principles that normally serve as guideline for every flight:

- The recording of atmospheric measurements is started as soon as the balloon approaches the stratosphere. During ascent of the balloon the atmosphere is observed in an upward-looking mode with 2 or 3 successive elevation angles of typically 7 to 2 degrees above the local horizon.
- At float 1 to 2 complete limb sequences are obtained in a stepwise scanning mode with a typical stepsize of 2 – 3 km. At each elevation angle several interferograms are taken. The number of interferograms on each elevation angle increases with the height of the tangent point to compensate partly for the reduced emitted energy at higher altitudes.
- Calibration measurements consisting of blackbody and so called ‘deep space’ (elevation angle: +20 degree) measurements are taken at the beginning and at the end of each limb scan sequence.
- The azimuth angle is adapted to the geophysical and/or illumination conditions in order to minimise gradients of the geophysical parameters along the line-of-sight.

The measurement scenario as performed during the flight of the MIPAS-B2 instrument at Aire sur l’Adour in May 1998 (MIPAS-B2 flight No.6) is shown below:

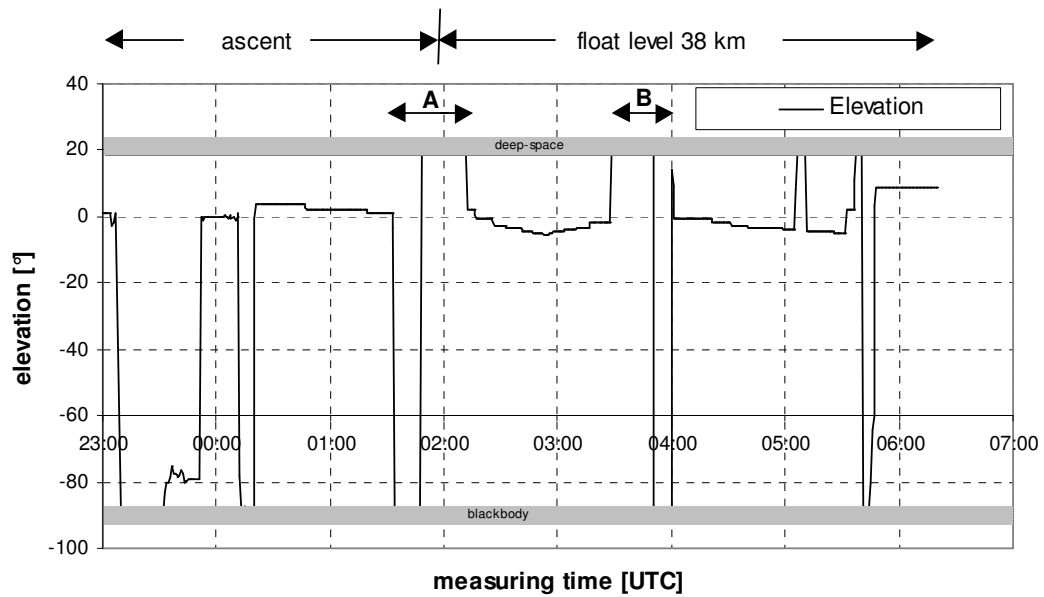


**Fig. 1** Measuring scenario of the MIPAS-B2 flight on 8.5.1998 at Aire sur l'Adour. The limb sequence is taken between the calibration cycles (A) and (B). The calibration cycles comprise each a blackbody and a deep-space measurement.

The first limb sequence (between the calibration cycles A and B) from MIPAS-B flight No. 6 was selected within the framework of this study. For further information concerning the flight see [Frie1999-2].

## 4. Definition of the data levels

This report describes the data processing from data level 0 to data level 1b.

The data levels for the MIPAS-ENVISAT experiment are defined in the technical notes of ESA Level 1B data definition [LEVEL1B] and in the report of the 'Data Processing and Algorithm Development Subgroup' [DPAD1995]:

*'The first two steps (level 0 to 1b) are mainly concerned with error correction and restoration of interferograms as well as with the transformation of these corrected interferograms into localised and calibrated spectra.'*

Level	Data Product Output	Essential Auxiliary Data
0	Raw MIPAS data	
1a	<ul style="list-style-type: none"> <li>- Quality checked interferograms from individual channels</li> <li>- Calibrated instrument auxiliary data (e.g. blackbody temperature, interferogram sampling information)</li> </ul>	
1b	<ul style="list-style-type: none"> <li>- Localised, radiometrically and frequency-calibrated spectra</li> <li>- ILS data</li> <li>- NESR assessment data</li> <li>- Processed &amp; validated calibration data (offset, gain)</li> <li>- others</li> </ul>	location of tangent points, instrumental housekeeping data

**Tab. 1** Data product definition

## 5. Description of the processing chain

The interferograms were sampled with the following parameters:

	Channel 1	Channel 2	Channel 3	Channel 4
<b>MIPAS-B2 instrument</b>				
Max. optical path difference	14.5 cm			
$\lambda_{\text{Laser}}$	0.632991366 $\mu\text{m}$			
$\sigma_{\text{Nyquist}}$	7899.00188 $\text{cm}^{-1}$			
Undersampling factors	15	9	17	6
Sampling interval	9.495 $\mu\text{m}$	5.697 $\mu\text{m}$	10.761 $\mu\text{m}$	3.798 $\mu\text{m}$
Numerical spectral range	526.600 .. 1053.200 $\text{cm}^{-1}$	877.667 .. 1755.334 $\text{cm}^{-1}$	1393.942 .. 1858.589 $\text{cm}^{-1}$	1316.500 .. 2633.001 $\text{cm}^{-1}$
Delivered spectral range	685.0 .. 969.975 $\text{cm}^{-1}$	1020.0 .. 1499.975 $\text{cm}^{-1}$	1570.0 .. 1749.975 $\text{cm}^{-1}$	1820.0 .. 2409.975 $\text{cm}^{-1}$

**Tab. 2** Comparison of the spectral ranges of MIPAS-B2.

The routine processing is performed on ground. The data processing up to level 1b is concerned with the transformation of the interferograms into calibrated and localised spectra. A dataflow diagram is given in Fig. 2 indicating the individual processes and their input/output data products.

The initial part of the processing chain is identical for atmospheric data, deep-space (offset) and blackbody (gain calibration) data. The major tasks during the generation of spectra are as follows:

- The interferograms are checked for consistency with respect to sampling errors, spikes, noise and instabilities of elevation angles during the scan. Erroneous interferograms are discarded.
- If the interferometer is running in a very stable mode which leads to a constant linear phase, interferograms of the same line of sight (LOS) can be co-added within a limited time interval to reduce the impact of noise by preserving the correct phase information.
- IFGs recorded for the individual spectral channels are transformed into complex spectra,
- The individual phase of each IFG is calculated.
- The interferograms are corrected by using the phase information.
- The phase-corrected IFGs are transformed into (apodized) spectra.
- The offset (deep-space) spectra are subtracted from the atmospheric ones.

- The gain calibration is performed by using the blackbody spectra with the associated blackbody temperature and the deep-space spectra.
- The spectral calibration (errors due to laser frequency instabilities and drifts) is performed.
- The determination of the instrumental line shape (ILS) is calculated by modelling the detector field-of-view distribution. The ILS is parameterised according to this distribution for any spectral position.

For calibration purposes three types of spectra are processed (Fig. 2):

- the atmospheric raw spectra,
- the blackbody raw spectra for gain calibration and
- the “deep-space” raw spectra for offset and gain calibration.

These three types of spectra are processed differently and therefore will be discussed separately. Co-addition of interferograms for "deep-space" measurements and co-addition of spectra for blackbody measurements is performed to reduce the noise level. The pairs of calibration measurements prior and after the limb scan are interpolated at that time the individual scene spectra were obtained.

In the following all processes will be briefly described together with their parameterisation in the sequence as they are performed within the processing chain during level 1b data processing. Each of the four MIPAS-B2 channels were processed and parameterised individually.

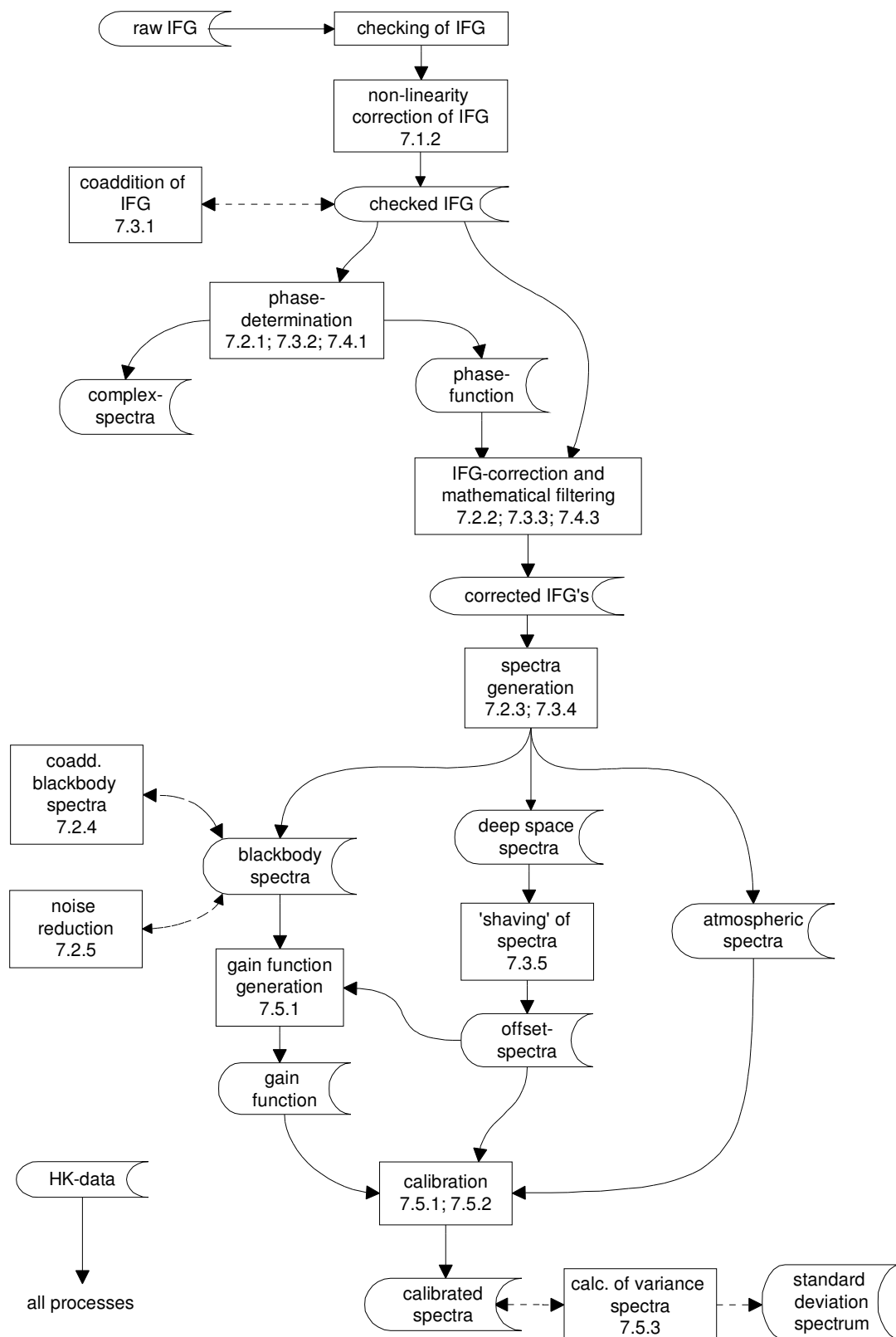


**Fig. 2:** Dataflow diagram of the MIPAS-B2 data processing chain (apodisation can be switched on at every generation of a spectrum). The numbers in the boxes indicate the subsections, in which these processes are described in more detail.

## **6. Overview of the processing algorithms of MIPAS-B2**

### **6.1. Differences between MIPAS-B2 and MIPAS/ENVISAT data processing**

In the case of MIPAS/ENVISAT high resolution offset measurements are not necessary since the observing geometry for the 'deep space' measurements precludes any atmospheric signal. Therefore no residual atmospheric lines have to be removed from the transformed 'deep' space spectra. This, together with the assumption that the linear phase is supposed to be absolutely stable for the satellite instrument except for instabilities caused by sampling errors, allows to use the phase correction scheme as proposed by Revercomb [Reve1988]. This method includes the phase correction within the gain calibration.

Scene measurement and gain calibration data are corrected first for the instrument self emission by subtracting the previous offset interferogram from the measured scene interferogram. Next, the complex Fourier transform is computed to yield a spectrum. This complex spectrum is then divided by the previous gain spectrum, which is also complex and shows ideally the same imaginary components as the scene data. A gain spectrum acts as reference for all subsequent scene data. Thus, the division by the gain spectrum rotates the complex components back into the real plane, and the resulting spectrum is supposed to be radiometrically calibrated as well.

In the 'deep space' measurements of MIPAS-B2 atmospheric lines from molecules above the balloon are present in certain frequency regions. Therefore, the offset calibration of MIPAS-B2 data has to be treated differently from the MIPAS-ENVISAT data processing.

MIPAS-B2 is designed as a two port interferometer whereas MIPAS-ENVISAT has a four port design. The spectral bands of the MIPAS-B2 experiment were adapted to the spectral bands of the MIPAS/ENVISAT as closely as possible [Frie1999-2].

Since the linear phase has to be constant with an accuracy of better than  $5 \cdot 10^{-2}$  rad [Trie2000] to assure that the error due to the calibration is smaller than the NESR, the absolute stability of the linear phase is not assumed for MIPAS-B2. To get the required data phase quality, the phase has been handled very carefully. Therefore, the interferograms are recorded double-sided.

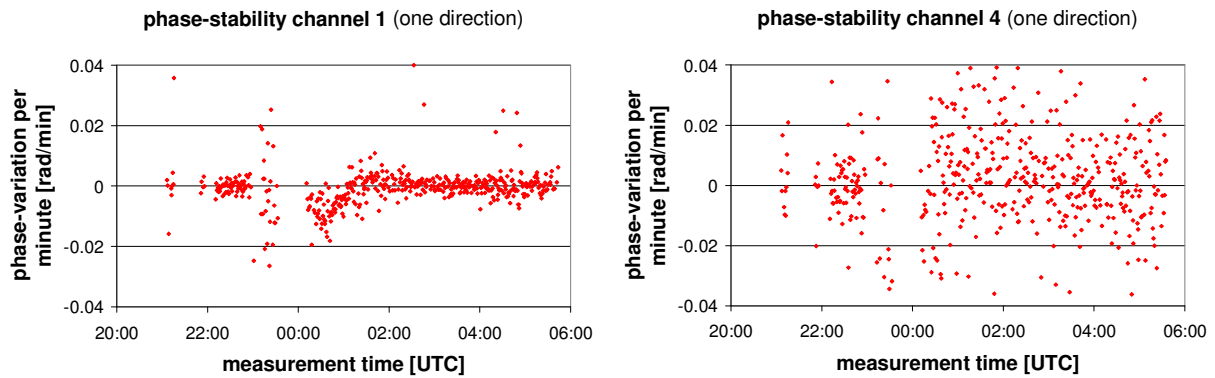


**Fig. 3:** Variation of the linear phase of consecutive measurements for channel 1 (left side) and channel 4 (right side).

## 6.2. Phase correction of interferograms

In Fourier spectroscopy an ideal Michelson interferometer would lead to fully symmetrical interferograms. Because the spectrum is the Fourier transform of the interferogram, the spectrum would then be real. Any asymmetry of the interferogram causes a complex spectrum, which is the case for all real Michelson interferometers due to sampling shifts and the instrumental phase which originates in the optical components and layout of the instrument. In the complex plane the phase of the spectra has to be corrected since radiation is a real quantity.

The balloon borne MIPAS-B2 spectrometer has been designed to restrict the instrumental background radiation by cooling the optics to about 210K. The low self-emission from each of the instrument ports leads to low photon loads and radiometrically balanced ports of the interferometer, especially in the long-wavelength channel when the instrument is looking at high tangent altitudes. The radiometric accuracy depends strongly on the quality of the phase correction of interferograms and on the calibration measurements and algorithms. It could be observed that the phases of the complex spectra derived by the standard method [Form1966] show line structures which are in correlation with line structures in the spectrum yielding distorted calibrated spectra. These phase functions cannot be explained by the instrumental phase due to optical or electrical components nor by sampling shifts but by the emission of the beamsplitter itself. The determination of the instrumental phase function requires to invent an unconventional technique.

Due to the low radiance received from the stratosphere, noise has also to be taken into account, especially in case of single non-co-added spectra. To be unaffected by noise in the phase spectra, an advanced statistical method was investigated for deriving the phase of the interferogram. The phase can be found by minimizing the correlation between the real and imaginary part of the spectrum as well as the variance of the imaginary part (the beamsplitter spectrum).

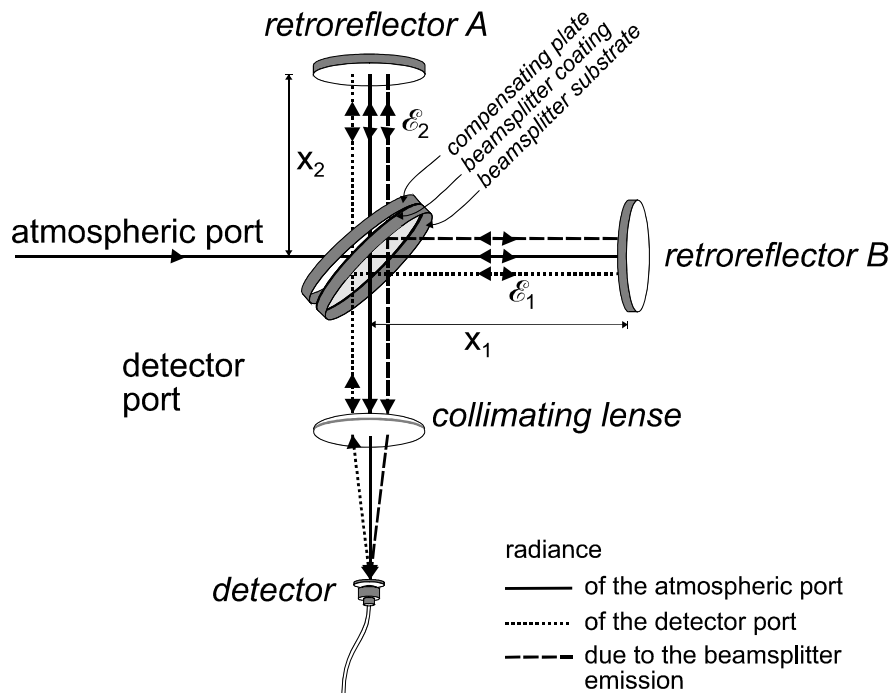


**Fig. 4** Idealized drawing of the interferometer showing the contributions of the different ports.

The radiation by the different sources enters the interferometer via two ports (Fig. 4). The main sources of radiation are the atmosphere and the reflection of the background radiation by the dewar window itself. Due to the different number of reflections the phases of those two sources differ by  $\pi$  in the complex spectrum. The self emission of the mirrors is much smaller than the latter sources. It is compensated in first order by the calibration. A third source of radiation is the beamsplitter emission itself, which has a phase angle of  $\pi/2$  [Wedd1993] to the atmospheric port and to the dewar port. Due to re-absorption of the radiation in the beamsplitter, the phase relation to the atmospheric port may vary a little from  $\pi/2$  for the beamsplitter emission and from  $\pi$  for the detector port. However, this effect can be neglected. Therefore, in the complex spectral plane the contribution of the atmospheric port is a real positive, of the detector port a real negative and of the beamsplitter emission an imaginary quantity, respectively. In the case that the atmospheric and the detector port become balanced, the beamsplitter emission even small becomes significant leading to a phase rotating together with the spectral structures in the complex plane. This effect is not equivalent to and cannot be described by the instrumental phase nor by the linear phase introduced by sampling shifts.

### 6.2.1. Methods for phase determination and correction for MIPAS-B2

The 'classical' approach of the phase correction [Form1966] was introduced to correct the interferogram for linear and instrumental phase by taking only the atmospheric port into account. In this case, the phase is derived by retrieving the angle between the real and imaginary part of the complex spectrum. This method is not suitable in our case, because it neglects the beam splitter emission.

The 'differential' phase correction [Wedd1993] takes this effect into account by defining the instrumental phase as the angle between the derivatives of the imaginary and real parts of the complex spectrum. However, noise in the differential spectra deteriorates the accuracy of the differential phase method, e.g. in case of single spectra and/or spectra at high elevation angles (Fig. 5).

With the a-priori assumption that the imaginary part of the spectrum, i.e. the beamsplitter emission, must not contain any sharp features a further phase determination method could be established. This method relies the following constraints:

- the correlation between the atmospheric and the beamsplitter spectrum has to vanish and
- the variance of the beamsplitter spectrum has to be minimised.

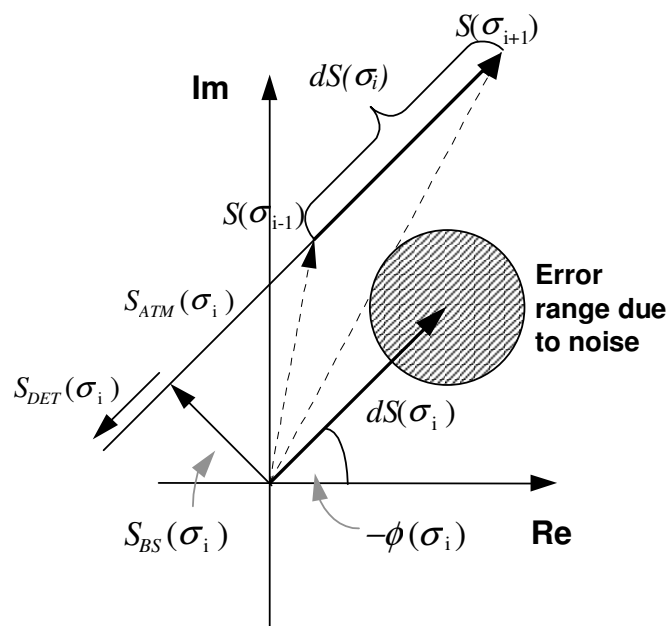


**Fig. 5** Schematic diagram of the components of a complex spectrum with the atmospheric ( $S_{ATM}$ ), the detector ( $S_{DET}$ ), the beamsplitter ( $S_{BE}$ ) emission and the differential spectrum  $dS$ . The circle illustrates the intensity and phase uncertainty due to noise.

This new approach of the phase determination is called 'statistical phase' determination [Trie2000]. The phase derived by the 'classical' or 'differential' method is corrected by using the following technique:

In case of a negligible magnitude of the beamsplitter and detector emission compared to the blackbody emission, the non-linear instrumental phase can be determined by a blackbody measurement. This instrumental phase  $\Phi^*$  is defined as the phase of the interferometer due to the emission of the beamsplitter and other optical and electrical components. Within a limited time interval in which the instrument is thermally stable, it can be assumed, that the instrumental phase  $\Phi^*$  will remain constant. This assumption is valid, because the thermal drift between two

calibration sequences of flight 6 was smaller than 2 K and therefore too small to change the beamsplitter emission significantly. The phase function  $\Phi$  can be developed around the phase  $\Phi^*$ .

The first element of the phase function  $\Phi = \Phi^* + \Delta\Phi$  describes the instrumental phase. The second element represents the residual phase error mainly introduced by sampling shifts. This invokes a linear phase error of the interferogram which can be assumed as

$$\Delta\Phi(\sigma) = a + b(\sigma - \sigma_0)$$

where  $\sigma_0$  is introduced as the centre of the spectral bandwidth to restrict numerical errors.

The back-rotation of the measured complex spectrum by  $e^{i(\Phi^* + \Delta\Phi)}$  turns the atmospheric portion of the spectrum parallel to the real axis. The corrected spectrum  $S$  can be written by using the developed phase function as:

$$\begin{aligned} S &= \bar{S} \times e^{i(\Phi^* + \Delta\Phi)} \\ &= \bar{S} \times \left[ e^{i\Phi^*} + ie^{i\Phi^*} \Delta\Phi + \dots \right] = S_{\Phi^*} + iS_{\Phi^*} \Delta\Phi + \dots \\ &= \text{Re}(S_{\Phi^*}) - \text{Im}(S_{\Phi^*}) \Delta\Phi + i \left[ \text{Im}(S_{\Phi^*}) + \text{Re}(S_{\Phi^*}) \Delta\Phi \right] + \dots \end{aligned}$$

with

$\bar{S}$  : measured complex spectra

$S$  : phase corrected spectra

The solutions for the parameters  $a$  and  $b$  of the linear phase error  $\Delta\Phi(\sigma)$  can be given by

1. the vanishing correlation between the real part of the corrected spectrum  $S$ , representing contributions from the atmospheric and detector ports, and the imaginary part, representing the beamsplitter emission. To suppress the influence of the correlation of the overall filter function, which is equivalent in the real and imaginary part, the spectra are highpass- filtered.

$$\begin{aligned} \mu &= \text{correl}(\text{Re}(S), \text{Im}(S)) \rightarrow \pm 0 \\ &= \sum_i \left[ \text{Re}(S_{\Phi^*,i}) - \text{Im}(S_{\Phi^*,i}) \Delta\Phi \right] \left[ \text{Im}(S_{\Phi^*,i}) + \text{Re}(S_{\Phi^*,i}) \Delta\Phi \right] \end{aligned}$$

The equation above converges rapidly for the phase offset  $a$ . But for the slope  $b$  the positive line correlations at one side of the spectral band might be compensated by negative line correlations at the other side. This might lead to a physically incorrect result. Therefore, only the offset  $a$  as derived from the correlation minimization will be used for updating the phase in this case.

2. the disappearance of any atmospheric features in the beamsplitter spectrum. To accomplish this the variance of the beamsplitter spectrum is minimized.

$$\begin{aligned}\frac{dv}{d(\Delta\Phi)} &= \frac{d \text{variance}(\text{Im}(S))}{d(\Delta\Phi)} = 0 \\ &= \frac{d \sum_i \left[ \text{Im}(S_{\Phi^*,i}) + \text{Re}(S_{\Phi^*,i}) \Delta\Phi \right]^2}{d(\Delta\Phi)}\end{aligned}$$

This equation converges well for the slope  $b$  but not for the offset  $a$ . The speed of convergence can be improved by squaring the argument in the sum leading to the minimization of the kurtosis.

$$\frac{d(v^2)}{d(\Delta\Phi)} = \frac{d \sum_i \left[ \text{Im}(S_{\Phi^*,i}) + \text{Re}(S_{\Phi^*,i}) \Delta\Phi \right]^4}{d(\Delta\Phi)} = 0$$

A solution is found if:

$$\begin{aligned}\frac{\partial(v^2)}{\partial a} &= 0 \\ \frac{\partial(v^2)}{\partial b} &= 0\end{aligned}$$

An important pre-condition for the rapid convergence of the  $\Delta\Phi$  is a good choice of the initial phase for the iteration process, where the above mentioned conditions are already satisfied within a specific error range. It was obtained during the data evaluation of MIPAS-B2 data that:

- A classical phase [Form1966] could be used as the boundary condition for the differential phase points which are distributed over an interval of  $\pi$  or directly as the initial phase guess for the statistical method.
- The differential phase is beneficial for the initial phase guess if the S/N of single spectral features is higher than  $\sim 10$  and spectral features are spread over the whole bandwidth.

For the initial phase the instrumental phase is fitted to the given 'classical' or 'differential' phase curve by adding a linear function onto the instrumental phase curve. The fit is weighted over the spectral axis with the intensity in the spectrum respectively with the absolute value of the first derivatives of the spectrum.

The back-rotation of the atmospheric and detector port contributions of the measured spectra  $\bar{S}$  to the real axis in the spectral domain is performed by correcting the individual or co-added IFG  $\bar{I}$ . The correction is done by convolution of the IFG with the Fourier transform of the function  $e^{i\Phi}$ ,

$$\begin{aligned}S &= \bar{S} e^{i\Phi} \\ \Downarrow \\ I &= \bar{I} \otimes \text{FT}^{-1}[e^{i\Phi}]\end{aligned}$$

The variation of the correlation and the kurtosis act as the stop criterion for the iterative process of the statistical phase determination. If the decrease of one parameter (vanishing correlation or minimised kurtosis) is less than a selected value, the optimisation is switched to the other criterion to optimise the phase. If the

improvement of both criteria is below the selected values, the iteration process is terminated. A maximum of 15 steps is sufficient to obtain a well behaved phase function.

Finally, the corrected interferograms are Fourier transformed to achieve the desired complex spectra.

$$S = FT^+[A(\bar{I} \otimes FT^{-}[e^{i\Phi}])]$$

The real and imaginary parts of the final spectra represent the atmospheric radiance subtracted by the detector port radiance and the beamsplitter's self-emission, respectively. The apodisation  $A$  in the equation shown above may be applied to limit the introduced 'ripples' due to the apparatus-function. The selection of the apodisation function is done according to the users choice. The description of apodisation is given in section 8.8. The quality of the phase correction can be assessed by analyzing the complex spectrum where the conditions as described above have to be satisfied.

Furthermore, the imaginary parts of the spectra have to remain invariant among all individual spectra within a time interval of thermal stability of the instrument. Ideally, the phase corrected spectrum exhibits only noise and beamsplitter emission in the imaginary part. Thus, one check for the quality of the spectra is the comparison of the imaginary parts of successive spectra.

## 6.2.2. Results

The different phase determination approaches are compared in the following figures.

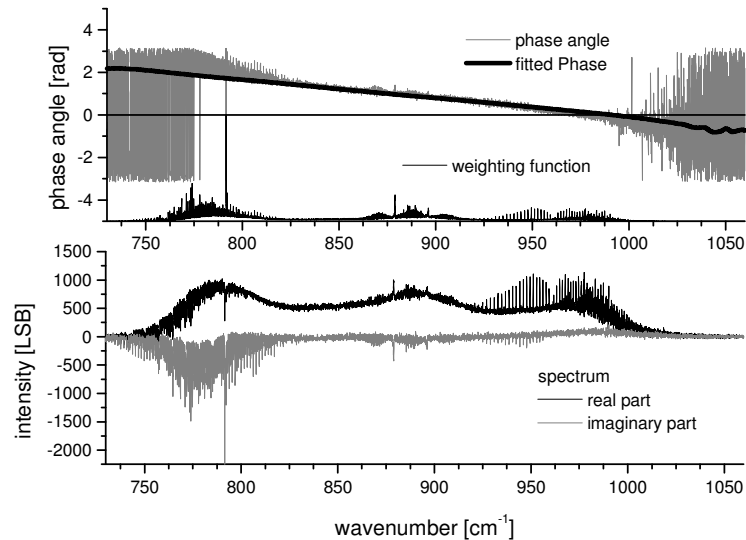


**Fig. 6** Outcome of the classical phase determination. The phase is fitted under the constraint of the weighting function. The atmospheric lines are distributed over the real and imaginary part. Therefore the energy is not preserved in the real part. The strength of the lines in the imaginary part is linked to the beamsplitter emission which is strong in the low wavenumber region (Fig. 7).

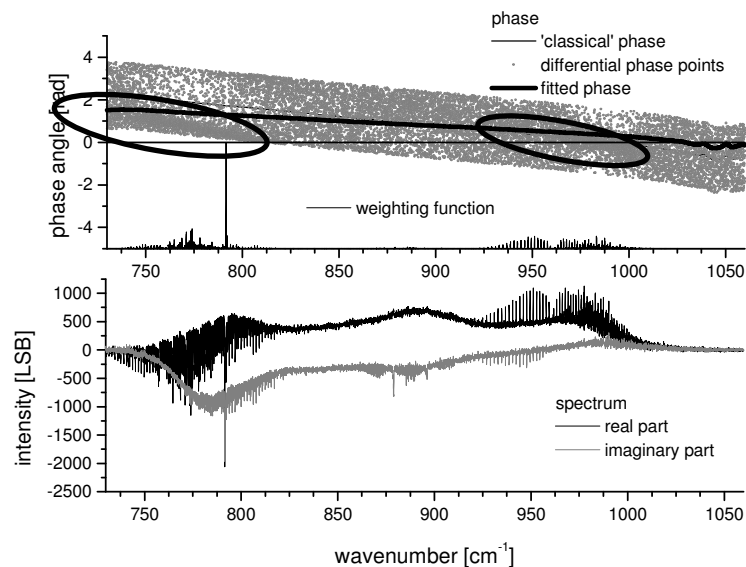


**Fig. 7** Outcome of the differential phase determination. Two heaps of phase points (circles) could be isolated. Due to the boundary condition of the phase band in the upper graph defined by the classical phase determination, a fit over all phase points leads to an insufficient differential phase determination though a weighting of the phase points was performed. Thus, the resulting spectra show signatures within the imaginary part.

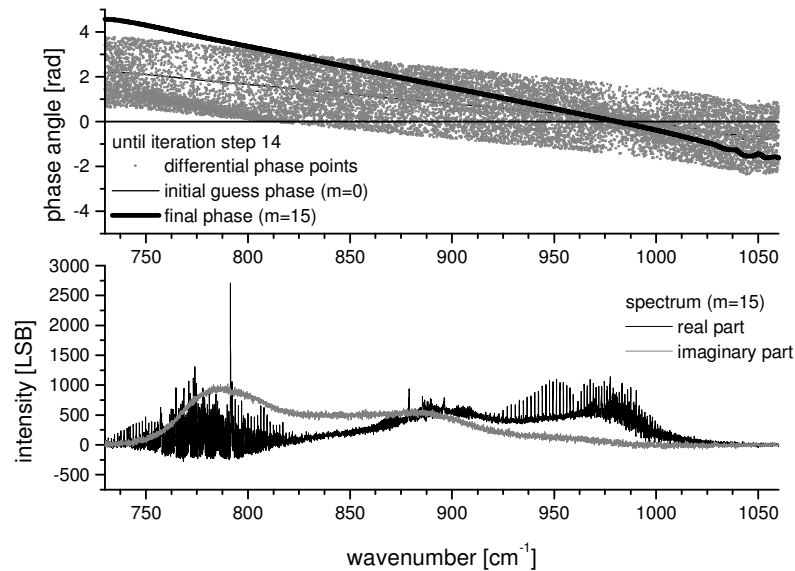


**Fig. 8** Outcome of the statistical phase determination approach. Result after 14 iteration cycles. The final phase is well above the heap of the differential phase points. The classical phase of figure 4 was used as initial guess phase for the iteration. In the imaginary part of the spectrum no more atmospheric lines appear.

### 6.3. Spectral and Radiometric Calibration

The calibration consists of two processes:

- Spectral calibration assigns values in wavenumber units ( $\text{cm}^{-1}$ ) to the abscissa, the wavenumber axis and
- radiometric calibration assigns values in spectral radiance units ( $\text{W}/\text{sr cm}^2 \text{cm}^{-1}$ ) to the ordinate, the intensity axis.

The spectral calibration is in first order obtained by the exact knowledge of the distance of the IFG sampling. The main causes for spectral calibration errors, which lead to a linear stretching/compression of the abscissa, are

- interferogram sampling errors by uncertainty of the reference laser frequency,
- the finite FOV and inhomogeneous illumination (only stretching),
- misalignment of the interferometer, and
- residual non-linear shift error, which are assumed to be very small compared to the linear errors.

The overall spectral errors have been determined by sharp molecular lines with high S/N-ratio in high tangent altitudes spectra. A linear spectral error function was fitted to the retrieved frequency shifts and according to this function the abscissa were corrected.

The radiometric calibration is obtained by subtracting the instrumental offset from the atmospheric spectra and applying a gain calibration function to these values.

This purpose requires various additional interferograms/spectra to be recorded for

- offset calibration: observation of the ‘cold space’ to determine the radiation emitted by the instrument itself,
- gain calibration: with the offset corrected spectrum of the internal calibration blackbody source of known temperature, the gain-function can be defined. With this function the uncalibrated spectra are converted into physical units of spectral radiance.

$$S_{\text{calib}} = (S_{\text{atm.}} - S_{\text{offset}}) \times \underbrace{\left[ \frac{S_{\text{BB}} - S_{\text{offset}}}{S_{\text{Planck}}} \right]^{-1}}_{\text{Gainfunction}}$$

Offset calibration is performed several times per flight to account for temperature drifts of the instrument. The ‘deep space’ measurements at +20° elevation angle are performed at full resolution and are co-added to reduce the noise level. The high resolution is necessary to resolve residual atmospheric lines from airmasses above the balloon altitude. To obtain the pure instrumental offset, residual sharp atmospheric lines are removed from the ‘cold space’ spectra (called ‘shaving’).

Calibration blackbody measurements are performed several times during ascent and at float level, each lasting 5 to 15 minutes. The temperature of the calibration blackbody provides the basis for the conversion of arbitrary units into absolute radiance units.

## 6.4. Localisation

The localization information of the tangent points is based on the pointing and star reference system of the MIPAS-B2 gondola and the GPS onboard-receivers [Mauc1999]. Each spectrum is localized in terms of time, position and altitude. The localization takes into account the atmospheric refraction of the line-of-sight for the real p/T profile on the day and time of the observation. For co-added spectra the localization and the measurement time are interpolated to a mean value. This is justified by the high degree of stability of the LOS fluctuations less than 0.5 arcmin/1σ for one nominal pointing angle [Frie1999]. During flight the acquisition and stabilization of the LOS is performed by an active pointing system that bases on a north seeking inertial navigation system with an embedded GPS [Seef1995].

## 6.5. ILS determination

It is possible but very tedious to retrieve the ILS of a FTS from laboratory measurements. Another approach is to approximate the ILS by the FOV distribution of the detector optics, which is the dominant factor for ILS broadening. If the mean intensity  $\bar{I}_\theta(\theta)$  of the FOV on a circle with an off-axis angle  $\theta$  is known, then the broadening function  $\bar{I}_{\sigma_0}(\sigma)$  can be determined. The instrument ILS can be calculated by convolution of the broadening function with the ideal ILS. The broadening function is obtained by substituting the angle  $\theta$  in  $\bar{I}_\theta(\theta)$  by a function of  $\sigma$  as:

$$\overline{I}_{\sigma_0}(\sigma) = \begin{cases} \overline{I}_{\theta} \left( \arccos \left( \frac{|\sigma|}{\sigma_0} \right) \right) & \text{if } \cos(\theta_{\max}) < \frac{|\sigma|}{\sigma_0} < 1 \\ 0 & \text{else} \end{cases}$$

Integrating of  $\overline{I}_{\theta}(\theta)$  over the FOV means integrating  $\overline{I}_{\sigma_0}(\sigma)$  from 0 to infinity to obtain the interferogram of a monochromatic source at wavenumber  $\sigma_0$ . After Fourier transformation one gets

$$S(\sigma) = \frac{2\pi\text{OPD}}{\sigma_0} \text{SINC}(2\pi\text{OPD}\sigma) \otimes \overline{I}_{\sigma_0}(\sigma) \propto \text{ILS}(\sigma)$$

which is just the definition for the ILS. It follows from the last equation, that the modulation function of the interferogram is just the Fourier transform of the broadening function  $\overline{I}_{\sigma_0}(\sigma)$ , normalized to one at ZOPD.

For the quantification of the FOV distribution a model was developed which characterizes the detector FOV of MIPAS-B2 from two cross sections of measurements which cut the FOV perpendicular (one meridional and one saggital slice) [Frie1999]. These slices are used to interpolate the FOV distribution for constant angles  $\theta$  by a cubic spline function. Fig. 9 shows the interpolated FOV distributions as obtained by this interpolation for all four channels. The obvious difference between channel one and the channels two to four is due a different detector optics. Channel one uses a cone for concentration of the beam, whereas for the other channels a lens optics is used.

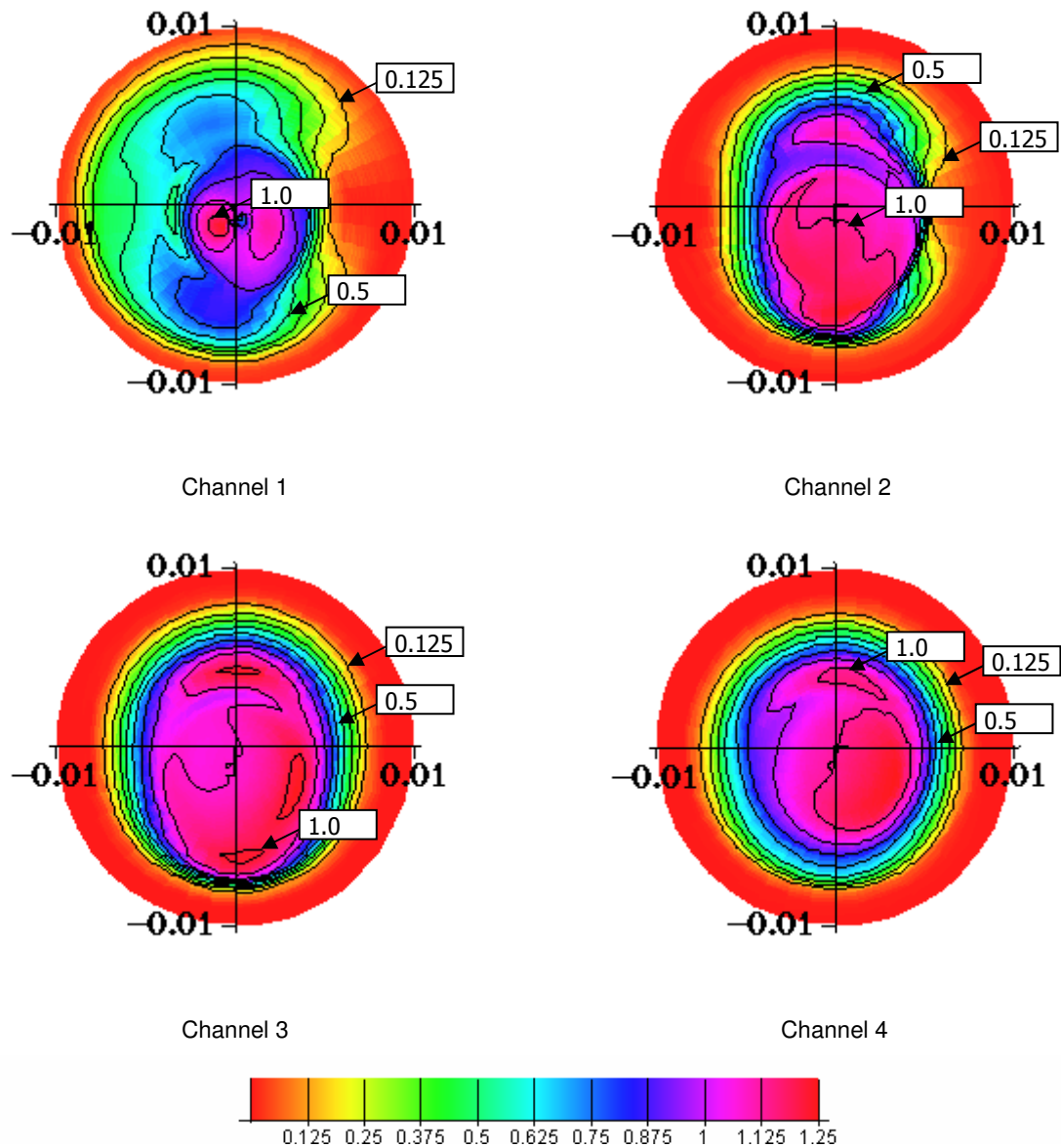


**Fig. 9** Model of the FOV-distributions for all four detector channels. The sagittal and meridional axis are scaled with the angle against the optical axis. The vertical axis corresponds to the vertical cross section of the telescope FOV.

From the FOV distributions for every channel a specific broadening function  $\bar{I}_{\sigma_0}^{-*}(\sigma)$  is obtained.

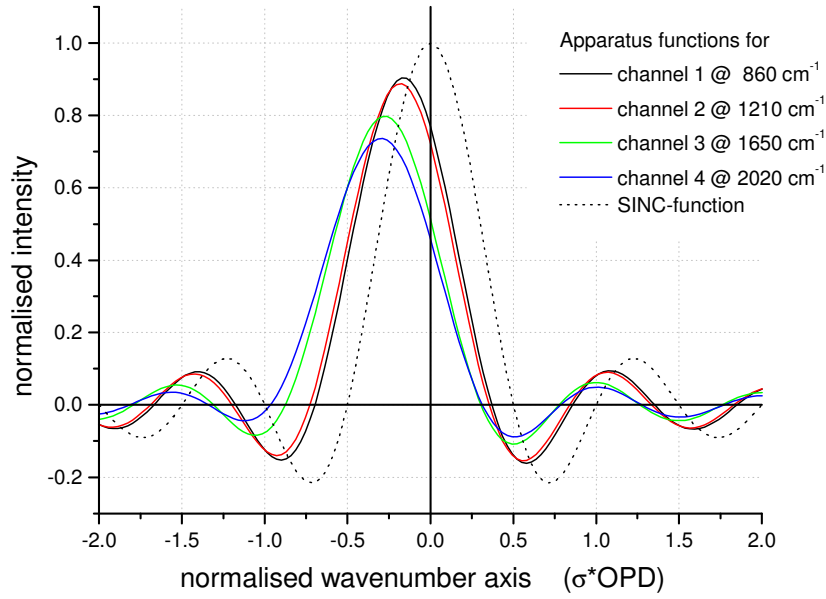


**Fig. 10** Modeled ILS for the four channels of MIPAS-B2.

The enlargement of the ILS due to the broadening function and an increasing spectral shift of the ILS toward lower wavenumbers  $\sigma_0$  can be seen in Fig. 10.

### 6.5.1. ILS parameterization

The ILS can be best described by parametrising the modulation function. With the parameterization of the modulation function the ILS can be calculated over the whole range of each spectral band. It is approximated by a power series

$$M(x) = \sum_{i=0}^4 \text{MOD}_i(x) = \sum_{n=0}^4 c_i \left[ 1 - \left( \frac{x}{\text{OPD}} \right)^2 \right]^i$$

whose terms can be Fourier transformed giving a set of Bessel functions. With the coefficients  $c_i$  the ILS can be derived by

$$\begin{aligned} \text{ILS}(\sigma) &= \sum_{i=0}^4 \left[ 2c_i \int_0^{\text{OPD}} \left[ 1 - \left( \frac{x}{\text{OPD}} \right)^2 \right]^i \cos(\sigma t) dt \right] \\ &= \sqrt{\frac{\pi}{2\sigma}} \sum_{i=0}^4 \frac{c_i \Gamma(i+1) \mathbf{J}_{(i+\frac{1}{2})}(\sigma)}{\left( \frac{\sigma}{2} \right)^i} \end{aligned}$$

$\Gamma$ : Gamma function  $\mathbf{J}$ : spherical Bessel functions

The parameters  $c_i$  are very smooth functions of  $\sigma_0$ . Therefore the  $c_i$  can easily be interpolated by a function of second order giving a defined ILS over the whole

spectral band. For each spectral band a set of  $c_i$  is supplied to account for differences in the FOV patterns.

## 6.6. Characterization of channeling

The physical origin of the channeling are Fabry-Perot interferences on parallel surfaces in the beam. In the case of MIPAS-B2, the responsible component is the detector itself. Back-illuminated Si:As-BIB detectors are used. The beam passes through the substrate of the detector before reaching the sensitive zone. Thus, the channeling can only be avoided by wedging the detector substrate. The only manufacturer of these detectors was not willing to consider this approach.

The strength of the channeling can be influenced by the optical coupling of the beam to the detector. The larger the divergence and the incidence angle of the incoming radiation bundle, the weaker the channeling pattern. In channel 1 a cone condenser which produces a large input divergence is used, in channel 2 to 4 a lens optics in combination with an incidence angle of  $27^\circ$  onto the detector is used to suppress the channeling patterns. (The strength of the feature is to a certain degree dependent on the distribution of energy within the beam, so it will vary slightly with the scene.)

The channeling is visible in channel 1 and 2; in channel 3 and 4 it is not identifiable. The amplitude is about 0.7% in channel 1 and 0.4% in channel 2 of the signal in the spectrum. Only one channeling 'frequency' with a period of  $3.86 \text{ cm}^{-1}$  was identified. These numbers were determined from coadded blackbody spectra, where the S/N is about 1000. The corresponding channeling feature is also clearly visible in the co-added blackbody interferogram. No other channeling features and no drifts in amplitude or frequency of the channeling feature larger than the noise can be identified within the limb sequence of flight 6.

Most of the channeling is removed in the calibration. Residual channeling for the spectra provided is below the NESR.

## 7. The parameterization of the individual processes

The routine processing of level 0 to 1b is performed on ground. The spectral ranges are given by the sampling interval and the Nyquist-theorem and are aligned to the bandwidth of the optical filters. The spectra are calculated in the following ranges:

	Channel 1	Channel 2	Channel 3	Channel 4
Numerical spectral range	660.0 .. 1000.0 cm <sup>-1</sup>	950.0 .. 1600.0 cm <sup>-1</sup>	1540.0 .. 1800.0 cm <sup>-1</sup>	1800.0 .. 2430.0 cm <sup>-1</sup>

### 7.1. Interferogram processing independent of the source

#### 7.1.1. Interferogram check

The initial part of the processing chain is identical for atmospheric data, deep-space (instrumental offset) and blackbody (gain calibration) data: the IFGs have to be checked for obvious errors like spikes by suitable algorithms. If errors are detected, the interferogram is marked and either corrected or discarded from the routine processing.

The removal of disturbed IFGs is necessary to assure the quality of the routine co-addition process as well as further processes. Distortions of the IFG are in that sense

- sampling errors,
- spikes in the IFG,
- changes of the LOS,
- any visual artefact (oscillations of the IFG-baseline, electronic distortions, etc ).

The limited number of IFGs during one flight of the MIPAS-Balloon experiment allows to perform this process interactively by comparing the interferograms respectively their quicklook magnitude spectra. Any of the above given distortions lead to obviously visible artefacts in the data products, so that no 'hard' threshold has to be defined for interactive controlling.

#### 7.1.2. Interferogram non-linearity correction

The gain function is defined by the relation between the detector current  $I$  and the incident power  $\phi$ . The derivative of the gain function represents the responsivity  $R$  (slope of the tangent of the gain function) around the mean value of the interferogram, respectively the mean incident power  $\phi$ . The gain function can be described by an allometric function  $I=a+b*\phi^c$ . The non-linearity errors due to the variation of the responsivity within the dynamic range of the interferogram are negligible for MIPAS-B2, so the non-linearity can be corrected by the reverse of the responsivity function.

$$IFG_{\text{corr}} = \frac{IFG_{\text{raw}}}{R_{(I)}} \quad \text{and} \quad R_{(I)} = bc \left[ \frac{I-a}{b} \right]^{\frac{c-1}{c}}$$

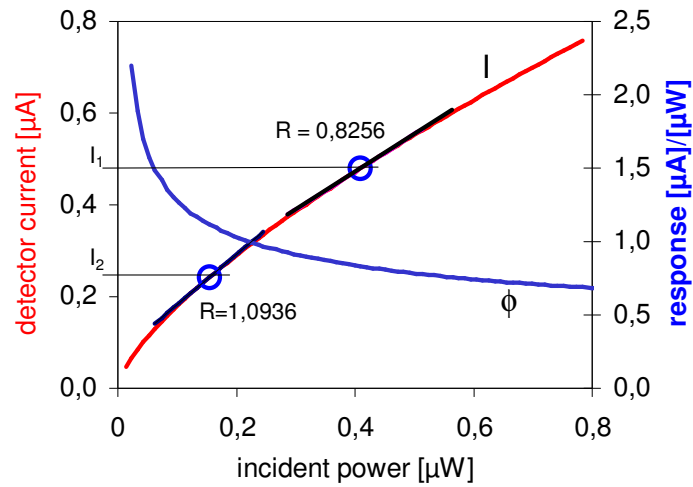


**Fig. 11** Gain function (detector current vs. incident power) between 7.4 and 8.4  $\mu\text{m}$  (red). The responsivity expressed by the derivative of the current of the incident power is shown in blue.

Non-linearity parameterization of of 6<sup>th</sup> flight of MIPAS-B2:

	Channel 1	Channel 2	Channel 3	Channel 4
a	-0.0078	-0.06168	-0.00984	-0.10553
b	64212.31	119694.53	2066131.63	2908910
c	0.86281	0.81525	0.94182	1.0

## 7.2. Blackbody spectra

The blackbody spectra are necessary to determine the calibration function for radiometric calibration of the atmospheric spectra. Due to the high signal-to-noise ratio these spectra can also be used to determine the instrumental phase.

Two blackbody sequences were analyzed: one before (A) and one after (B) the limb sequence.

### 7.2.1. Phase determination of blackbody interferograms

The phase is obtained by the angle between the real and imaginary part of the complex spectrum  $S(\sigma)$  (classical approach by [Form1966]). The spectrum is derived by a FFT from the interferogram IFG(x) which is degraded by the apodisation function  $A(x)$ .

$$S(\sigma) = \text{FT}^+ [A(x) \text{IFG}(x)]$$

$$\phi(\sigma) = \arctan \left[ \frac{\text{Im}(S(\sigma))}{\text{Re}(S(\sigma))} \right]$$

Resolution of blackbody spectra	1.0 cm <sup>-1</sup>
Length of interferogram (OPD) used	+/- 0.5 cm
Apodisation	Norton-strong

The output of this processing step is the “instrumental phase function” which is used as input for the phase correction of deep space and atmospheric spectra.

*Applied algorithms:*

8.11.1 ‘Classical’ phase determination

### 7.2.2. Interferogram phase correction

The phase disturbed interferogram shall be corrected such that the desired spectrum is purely real.

$$\text{IFG}_{\text{corr}}(x) = \text{IFG}(x) \otimes \underbrace{\text{FT}^{-1} \left[ e^{i\Phi(\sigma)} \right]}_{k^*(x)}$$

The correction kernel  $k(x)$  is optimised by the tapering function  $A(x)$  to reduce the wiggles of the Gibb’s phenomena. The tapering function can be any apodisation function.

$$k_{(x)} = k^*(x)A(x)$$

The corrected IFG is generated by a convolution of the disturbed IFG with the kernel  $k(x)$ .

$$\text{IFG}_{\text{corr}}(x) = \text{IFG}(x) \otimes k(x)$$

Kernel size	2048 points
Tapering function	Norton-strong

*Applied algorithms:*

8.9 Interferogram correction and mathematical filtering

### 7.2.3. Generation of blackbody spectra

The spectrum is derived from a real FFT of the corrected interferogram  $\text{IFG}_{\text{corr}}(x)$  which is tapered by the apodisation function  $A(x)$ .

$$S(\sigma) = \text{FT}^+ \left[ A(x) \text{IFG}(x) \right]$$

When applying phase corrected IFGs for spectrum generation, the real and imaginary parts of the spectrum can be explained as the scene and the beamsplitter-

self-emission, respectively.

$$S_{SC}(\sigma) = \text{Re}[S(\sigma)]$$

$$S_{ST}(\sigma) = \text{Im}[S(\sigma)]$$

Resolution of blackbody spectra	0.0345 cm <sup>-1</sup> (Channel 1+3) 1.0 cm <sup>-1</sup> (Channel 2+4)
Length of interferogram (OPD) used	+/- 14.5 cm (Channel 1+3) +/- 0.5 cm (Channel 2+4)
Apodisation	Norton-strong (Contract 11717_95_NL_CN) Rectangle (Contract 12078_96_NL_GS)

Since some water vapor and CO<sub>2</sub> still remained in the instrument, their related narrow lines can be found in the blackbody spectra of channel 3 and of channel 1, respectively. This requires to calculate the blackbody spectra at highest resolution for channel 1 and 3 whereas the resolution can be reduced to increase the signal-to-noise in channels 2 and 4.

*Applied algorithms:*

8.7      *Generation of spectra*

#### 7.2.4. Co-addition of blackbody spectra

Co-addition in the spectral domain is performed to reduce the noise. The result of this procedure is equivalent to the co-addition of the interferograms. The spectra are already based on phase corrected IFGs. Therefore phase instabilities can not degrade the co-added data product. The noise is reduced by the square root of the number of co-added spectra. For co-addition in the spectral domain all spectra have to be on the same spectral grid.

Number of co-added spectra (sequence A)	18
Number of co-added spectra (sequence B)	22

*Applied algorithms:*

8.3      *Co-addition of spectra*

#### 7.2.5. Noise reduction in blackbody spectra (only channel 3)

Residual water vapour inside the instrument causes lines in channel 3 blackbody spectra. Therefore, the blackbody spectra could not be processed at lower spectral resolution to reduce the noise in the spectra. To reduce the noise by keeping the lines, the narrow H<sub>2</sub>O lines were removed before noise reduction and reinserted

afterwards. In channel 1 this procedure was not necessary due to the high signal-to-noise ratio of the blackbody spectra.

Resolution of spectrum prior to shaving	0.0345 cm <sup>-1</sup>
Intermediate resolution after shaving	1.0 cm <sup>-1</sup>
Resolution of spectrum at line positions after shaving	0.0345 cm <sup>-1</sup>

*Applied algorithms:*

8.13 'Shaving' - Removal of residual atmospheric lines in deep space spectra

### 7.3. Deep-space spectra

The „deep-space“ spectra are used for offset calibration. With an elevation angle of 20° upwards, broadband emission features from the atmosphere can be neglected. Therefore any broadband feature in the spectrum originates from the instrumental background emission. Lines in the deep-space spectra are due to atmospheric emissions of mainly CO<sub>2</sub> and H<sub>2</sub>O above the balloon altitude. These lines have to be eliminated during calibration.

Two deep-space sequences are analysed: one before (A) and one after (B) the limb sequence.

#### 7.3.1. Co-addition of deep-space interferograms

Co-addition of IFGs is performed to reduce the statistical noise in the interferogram introduced by photon or detector noise. In first order approximation, the noise can be reduced by the square root of the number of co-added IFGs.

Co-addition means an addition of single consecutive IFGs on exactly the same OPD grid. This can be guaranteed only if the instrument is working in an absolutely stable mode, i.e. no phase fluctuations occurred within the time-interval of co-addition. The fluctuations can be evaluated by the stability of the linear phase as explained in subsection 8.2. IFGs of different calibration sequences are not co-added.

For assigning time to the co-added IFGs the mean value of the measuring time of individual IFGs is used. The individual times of the IFGs are taken at ZOPD.

POPD (peak position of the IFG)	Determined by the IFG-Maximum
Number of co-added interferograms (sequence A)	Forward: 28 Backward: 28
Number of co-added interferograms (sequence B)	Forward: 28 Backward: 28

The preceding steps are performed separately for the interferograms taken at forward and backward movement of the interferometer, respectively.

*Applied algorithms:*

8.2 Co-addition of interferograms

### 7.3.2. Phase determination of deep-space spectra

The quality of the phase determination is enhanced by applying the statistical phase determination approach described in detail in chapter 6.2.

The complex spectrum used in all steps of this phase determination method is derived by a classical real FFT from the interferogram  $I(x)$  which is degraded by the apodisation function  $A(x)$ .

$$S(\sigma) = \mathbf{FT}^+ [A(x) \text{IFG}(x)]$$

A high-pass digital filtering is performed by convolution of the spectrum with a kernel function describing the filter.

The kernel represents the coefficients of a non-recursive, digital filter for evenly spaced data points. The kernel coefficients are Kaiser-weighted. The intensity of the Gibbs phenomenon wiggles are defined in -db; a value of 50 or more should be appropriate.

order of the kernel	20			
reduction of the Gibbs phenomena	50 dB			
lower frequency of the filter in fractions of the Nyquist frequency	0.4			
low wavenumber of bandwidth interval	660 cm <sup>-1</sup>	1000 cm <sup>-1</sup>	1540 cm <sup>-1</sup>	1720 cm <sup>-1</sup>
high wavenumber of bandwidth interval	980 cm <sup>-1</sup>	1600 cm <sup>-1</sup>	1800 cm <sup>-1</sup>	2500 cm <sup>-1</sup>
instrumental phase function	As defined in subsection 7.2.1			
max. residual uncertainty of the phase for iteration stop	20mrad			
Maximum number of iterations	25			

*Applied algorithms:*

8.11.3 Statistical phase determination

### 7.3.3. Phase correction of deep-space interferograms

→ See subsection 7.2.2, but the phase information is taken from the process described in the preceding section 7.3.2

### 7.3.4. Generation of deep-space spectra

The same processes are used as described in the section about blackbody spectra, (see subsection 7.2.3). The parameterisation is listed below:

Resolution of deep space spectra	0.0345 cm <sup>-1</sup>
Length of interferogram (OPD) used	+/- 14.5 cm
Apodisation	Norton-strong (Contract 11717_95_NL_CN) Rectangle (Contract 12078_96_NL_GS)

*Applied algorithms:*

8.7      *Generation of spectra*

### 7.3.5. Shaving of deep-space spectra

The "shaving" of spectra is necessary to remove any sharp spectral lines from the deep space spectra that are formed in the atmosphere above the balloon. The "shaving" is performed in the same manner as the "shaving" of blackbody spectra described in subsection 7.2.5, but in case of deep space spectra the lines are not reinserted afterwards.

The instrumental contribution to lines in the deep-space spectra can be neglected since their influence in the calibration procedure is of second order.

Resolution of spectrum prior to shaving	0.0345 cm <sup>-1</sup>
Resolution of spectrum after shaving	1.0 cm <sup>-1</sup>

*Applied algorithms:*

8.13      *'Shaving' - Removal of residual atmospheric lines in deep space spectra*

## 7.4. Limb sequence spectra

For the processing of the limb spectra, the first three steps are identical to the processing of deep space spectra, so for

### 7.4.1. Phase determination of limb sequence spectra

→ See subsection 7.3.2

### 7.4.2. Phase correction of limb sequence interferograms

→ See subsection 7.2.2

### 7.4.3. Generation of limb sequence spectra

→ See subsection 7.3.3

## 7.5. Calibration

### 7.5.1. Radiometric calibration of limb spectra

The radiometric calibration allows to convert the uncalibrated values into physical units of spectral radiance as described in Subsection 6.3. A two point calibration is performed. One calibration point is the offset spectrum  $S_{instr}$ , which is determined from 'shaved' deep-space spectra. The other calibration 'point' is a spectrum of the relatively 'hot' blackbody ( $S_{BB}$ , ~210K). Offset and blackbody spectra are interpolated to the time of the atmospheric measurement. Since all spectra are already phase corrected the individual phase relation of the interferograms has no significance.

The emissivity of the blackbody is characterized by  $0.9986 \pm 0.0006$ . This leads together with an uncertainty of the temperature measurement to an uncertainty of gain calibration of maximal  $0,23\% \pm 0,43\%$  [Trie2000 (The temperature gradient along the blackbody cylinder is negligible)].

At spectral positions of line features in the blackbody spectra the error budget is significantly higher. Therefore these spectral positions should be omitted for the retrieval of p, T and trace gases. A list of these spectral positions is given in Appendix 10.1

*Applied algorithms:*

8.12 *Radiometric calibration of the spectra*

	Channel 1	Channel 2	Channel 3	Channel 4	
Radiance of the blackbody					
$L_{BB}(T=220K)$	$4,5 \cdot 10^{-6}$ - $1,9 \cdot 10^{-6}$	$1,7 \cdot 10^{-6}$ - $3,0 \cdot 10^{-7}$	$1,5 \cdot 10^{-7}$ - $6,8 \cdot 10^{-8}$	$5,6 \cdot 10^{-8}$ - $1,9 \cdot 10^{-8}$	$\frac{W}{cm^{-1} sr cm^2}$
Absolute noise of the baseline					
Error due to noise in the blackbody spectra in the limb spectra $\Delta L_{ATM,NESR}$	<b><math>7 \cdot 10^{-9}</math></b>	<b><math>2 \cdot 10^{-9}</math></b>	<b><math>3 \cdot 10^{-9}</math></b>	<b><math>2 \cdot 10^{-9}</math></b>	$\frac{W}{cm^{-1} sr cm^2}$
Error due to phase inaccuracies in the limb spectra. $\Delta L_{ATM,\varphi_{ATM}}$	$\Delta\varphi_{tot,ATM} =$ $0,002 (710cm^{-1})$ .. $0,023 (1000cm^{-1})$	$\Delta\varphi_{tot,ATM} =$ $0,0008 (1040cm^{-1})$ .. $0,012 (1600cm^{-1})$	$\Delta\varphi_{tot,ATM} =$ $0,0095 (1641cm^{-1})$ .. $0,037 (1800cm^{-1})$		rad
	$7,4 \cdot 10^{-10}$ .. <b><math>1,4 \cdot 10^{-8}</math></b>	$3,7 \cdot 10^{-11}$ .. $5,0 \cdot 10^{-10}$	$3,1 \cdot 10^{-11}$ .. $7,7 \cdot 10^{-11}$	$3,7 \cdot 10^{-10}$	$\frac{W}{cm^{-1} sr cm^2}$
Error due to phase inaccuracies in the deep-space spectra. $\Delta L_{ATM,\varphi_{DS}}$	$\Delta\varphi_{tot,DS} =$ $0,003 (696cm^{-1})$ .. $0,050 (1000cm^{-1})$	$\Delta\varphi_{tot,DS} =$ $0,003 (1037cm^{-1})$ .. $0,059 (1600cm^{-1})$	$\Delta\varphi_{tot,DS} =$ $0,027 (1600cm^{-1})$ .. $0,086 (1800cm^{-1})$		rad
	$8,7 \cdot 10^{-10}$ - border of spectral range: <b><math>3,0 \cdot 10^{-8}</math></b>	$3,3 \cdot 10^{-11}$ - border of spectral range: <b><math>1,7 \cdot 10^{-9}</math></b>	$7,6 \cdot 10^{-11}$ - $1,4 \cdot 10^{-10}$	$3,7 \cdot 10^{-10}$	$\frac{W}{cm^{-1} sr cm^2}$
Geometric sum	$7,9 \cdot 10^{-9}$ - $3,3 \cdot 10^{-8}$	$2,0 \cdot 10^{-9}$ - $2,7 \cdot 10^{-9}$	$3,0 \cdot 10^{-9}$ - $3,0 \cdot 10^{-9}$	$2,1 \cdot 10^{-9}$	$\frac{W}{cm^{-1} sr cm^2}$
Rel. error of the baseline					
$\frac{\Delta L_{ATM,\varphi_{BB}}}{L_{ATM}}$	$S/N_{BB} = 1240$	$S/N_{BB} = 1730$	$S/N_{BB} = 235$	$S/N_{BB} = 63$	
	$6,9 \cdot 10^{-3}$	$1,5 \cdot 10^{-3}$	$8,3 \cdot 10^{-3}$	0,047	%

**Tab. 3** Budget of errors in the calibrated limb spectra due to noise in the data of the 6<sup>th</sup> flight of MIPAS-B2 on March 8, 1998.  $\Delta\varphi_{tot}$  represents the errors by the statistical phase determination. The beamsplitter emission can be neglected for channel 4. Therefore  $\Delta\varphi_{tot}$  is not available since the classical phase determination was used there.

## 7.5.2. Interpolation on the ENVISAT spectral grid and spectral calibration

The interpolation on the ENVISAT spectral grid of  $0.025 cm^{-1}$  is performed together with the spectral calibration for the following spectral ranges:

	Channel 1	Channel 2	Channel 3	Channel 4
Grid interval	$0.025 cm^{-1}$			
Spectral range	685.0 .. $969.975 cm^{-1}$	1020.0 .. $1499.975 cm^{-1}$	1570.0 .. $1749.975 cm^{-1}$	1820.0 .. $2409.975 cm^{-1}$

Spectral calibration has been obtained by retrievals in a set of spectral intervals distributed over the whole spectral range using the HITRAN database. From these retrievals the linear correction functions  $\sigma_{\text{corr.}} = c_0 + c_1\sigma_{\text{meas.}}$  have been determined. The coefficients of which and the standard deviation of the spectral shift values from the linear function are:

	Channel 1	Channel 2	Channel 3	Channel 4
$C_0$ [ $\text{cm}^{-1}$ ]	-0.05112	-0.0496435	-0.1318345	-0.05672
$C_1$	3.95771e-5	1.85948e-5	6.190211E-05	1.29845E-05
uncertainty of spectral calibration [ $\text{cm}^{-1}$ ]	5.3e-4	6.3e-4	2.6e-3	1.1e-3

### 7.5.3. Calculation of variance of single consecutive spectra

The standard deviation is calculated from consecutive calibrated spectra (subsection 7.5.2) of a certain elevation angle. The standard deviation corresponds to the overall instrument NESR which is photon noise limited. The variance, the diagonal elements of the variance/covariance matrix, is obtained by the square of the standard deviation values.

The off-diagonal elements of the covariance matrix are defined by the numerical apodisation function [Carlotti 1998] since the dominating noise in the interferogram is not affected by the self-apodisation. The total noise is dominated by the photon noise of the d.c. level which is of much larger intensity than the modulated part of the interferogram. Therefore the total noise does not correlate with the modulated part of the interferogram. This also means, that the magnitude of noise in the interferogram is constant over the whole optical path. Since this dominating noise in the interferogram is not affected by the self-apodisation, it is only modulated by the numerical apodisation function in the interferogram domain.

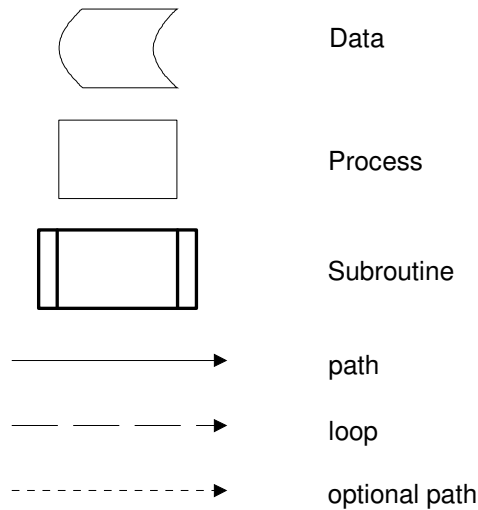
*Applied algorithms:*

8.8 *Generation of the variance of single consecutive spectra*

## 8. Algorithms - Reference

This chapter references the algorithms used for level 1b data processing for MIPAS-B2. The algorithms are listed in alphabetical order.

The following notation is used within the flowcharts:



In the tables for the definition of variables, the "I/O" (Input/Output) indication refers to the following notation:

Notation	Description
I	input of the process
loop	loop or index variable
t	temporary or intermediate variable
O	output of the process

In the same tables, the "Type" indication refers to the following notation:

Notation	Description
r	real number
d	date and time
c	complex number
i	integer number
o	ordinal number
t	text

## 8.1. Apodisation functions

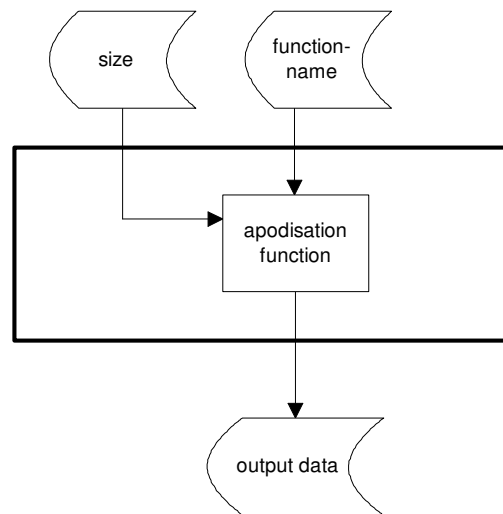
### Objective

The interferograms may be multiplied with apodisation functions generated within this subroutine to reduce the ripples of the SINC-function in the spectra originating from truncated IFG's.

Eight different apodisation functions are provided:

$A(x) = \left\{ \begin{array}{l} \sum_{i=0}^4 \alpha_i \left[ 1 - \left( \frac{x}{OPD} \right)^2 \right]^i \quad \sum_{i=0}^4 \alpha_i = 0 \\ \cos\left(\frac{\pi x}{2OPD}\right) + \alpha \cos\left(\frac{3\pi x}{2OPD}\right) \\ 1 + (1 + \alpha) \cos\left(\frac{\pi x}{OPD}\right) + \alpha \cos\left(\frac{2\pi x}{OPD}\right) \\ \text{RECT}\left[\frac{x}{2OPD}\right] \\ \left(1 - \left(\frac{x}{OPD}\right)^2\right)^2 \\ 1 - \frac{x}{OPD} \\ 0 \end{array} \right.$	Norton – Beer																								
	<table style="border-collapse: collapse; width: 100%; text-align: center;"> <thead> <tr> <th style="border-right: 1px solid black; padding: 5px;"></th> <th style="padding: 5px;">Strong (NS)</th> <th style="padding: 5px;">Medim (NM)</th> <th style="padding: 5px;">Weak (NW)</th> </tr> </thead> <tbody> <tr> <td style="border-right: 1px solid black; padding: 5px;"><math>\alpha_0</math></td> <td style="padding: 5px;">0.045335</td> <td style="padding: 5px;">0.152442</td> <td style="padding: 5px;">0.384093</td> </tr> <tr> <td style="border-right: 1px solid black; padding: 5px;"><math>\alpha_1</math></td> <td style="padding: 5px;">0</td> <td style="padding: 5px;">-0.136176</td> <td style="padding: 5px;">-0.087577</td> </tr> <tr> <td style="border-right: 1px solid black; padding: 5px;"><math>\alpha_2</math></td> <td style="padding: 5px;">0.554883</td> <td style="padding: 5px;">0.983734</td> <td style="padding: 5px;">0.703484</td> </tr> <tr> <td style="border-right: 1px solid black; padding: 5px;"><math>\alpha_3</math></td> <td style="padding: 5px;">0</td> <td style="padding: 5px;">0</td> <td style="padding: 5px;">0</td> </tr> <tr> <td style="border-right: 1px solid black; padding: 5px;"><math>\alpha_4</math></td> <td style="padding: 5px;">0.399782</td> <td style="padding: 5px;">0</td> <td style="padding: 5px;">0</td> </tr> </tbody> </table>		Strong (NS)	Medim (NM)	Weak (NW)	$\alpha_0$	0.045335	0.152442	0.384093	$\alpha_1$	0	-0.136176	-0.087577	$\alpha_2$	0.554883	0.983734	0.703484	$\alpha_3$	0	0	0	$\alpha_4$	0.399782	0	0
		Strong (NS)	Medim (NM)	Weak (NW)																					
	$\alpha_0$	0.045335	0.152442	0.384093																					
	$\alpha_1$	0	-0.136176	-0.087577																					
	$\alpha_2$	0.554883	0.983734	0.703484																					
	$\alpha_3$	0	0	0																					
	$\alpha_4$	0.399782	0	0																					
FillerD $\alpha=0.18$																									
FillerE $\alpha=0.18$																									
Rectangle(RE)																									
Tapering(TA)																									
Triangular(TR)																									
for $-OPD \leq x \leq OPD$																									
0 else																									

## Process flowchart



## Definitions of variables

Variable	Description	I/O	Type	Remarks
apod	apodisation function type	l	o	possible values: [NS, NM, NW, FD, FE, RE, TA, TR] default value := NS
i,z		t	i	
n	number of points of the interferogram to be apodised	l	i	n must be odd
A	apodisation function	O	r	
c	apodisation coefficients	t	r	array of 5 elements

## Algorithm

$$z = (n+1)/2$$

with  $i \in [0, z-1]$

$$\text{RE: } A_{z+i} = 1$$

$$\text{TR: } A_{z+i} = 1-i/z$$

$$\text{FD: } c_0 = 0.18$$

$$A_{z+i} = \cos\left(\frac{\pi i}{2z}\right) + c_0 \cos\left(\frac{3\pi i}{2z}\right)$$

$$\text{FE: } c_0 = 0.18$$

$$A_{z+i} = 1 + (1+c_0) \cos\left(\frac{\pi i}{z}\right) + c_0 \cos\left(\frac{2\pi i}{z}\right)$$

$$\text{TP: } A_{z+i} = [1-(i/z)^2]^2$$

$$\text{NW: } c = [0.384093, -0.087577, 0.703484, 0.0, 0.0]$$

$$A_{z+i} = c_0 + \sum_{j=1}^4 c_j [1-(i/z)^2]^j$$

$$\text{NM: } c = [0.152442, -0.136176, 0.983734, 0.0, 0.0]$$

$$A_{z+i} = c_0 + \sum_{j=1}^4 c_j [1-(i/z)^2]^j$$

$$\text{NS: } c = [0.045335, 0.0, 0.554883, 0.0, 0.399782]$$

$$A_{z+i} = c_0 + \sum_{j=1}^4 c_j [1-(i/z)^2]^j$$

and symmetrising:

$$A_{z-i} = A_{z+i}$$

$$A_0 = 0$$

## 8.2. Co-addition of interferograms

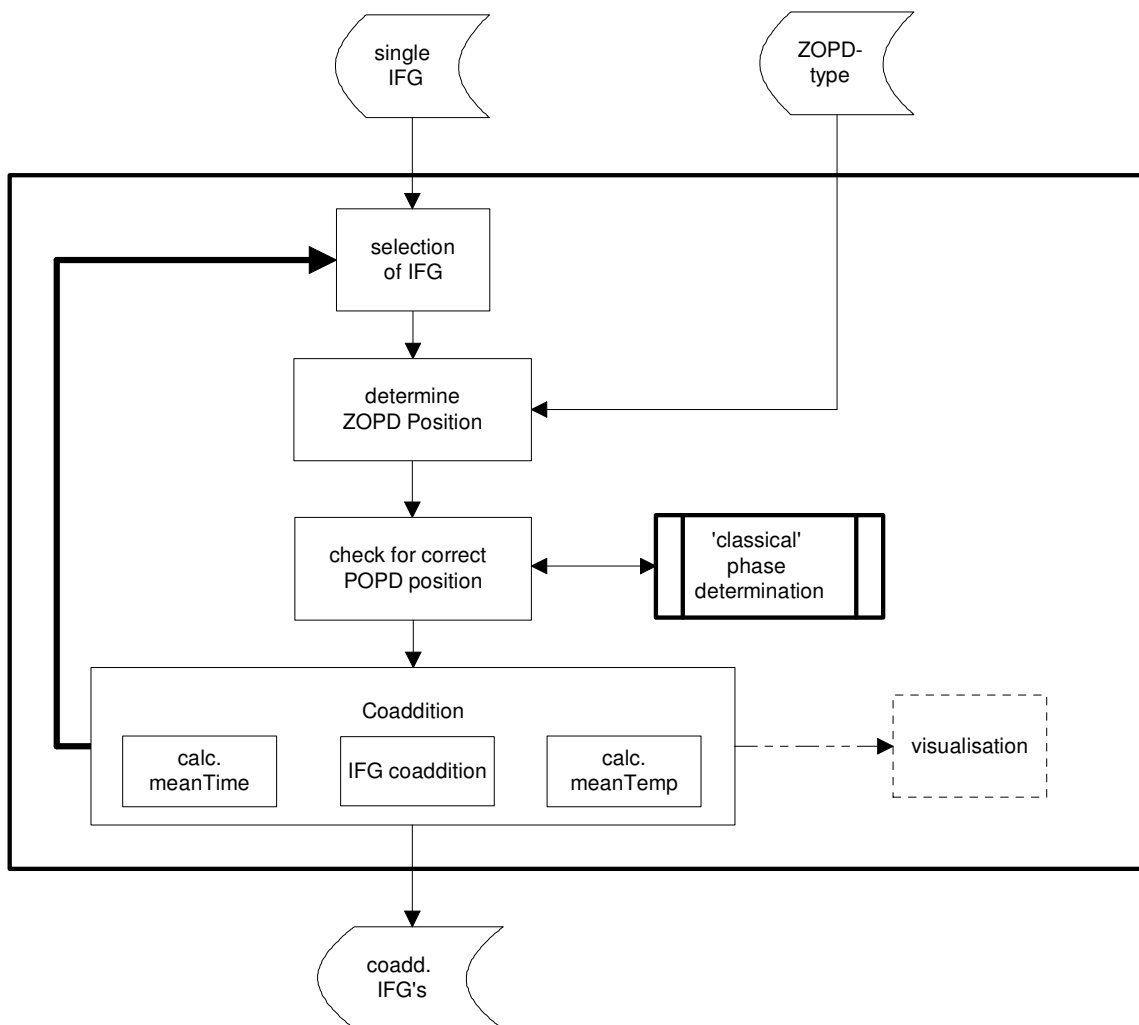
### Objective

Co-addition of IFGs is performed to reduce the statistical noise in the interferogram introduced by photon or detector noise. The noise is reduced by the square root of the number of co-added IFGs.

Co-addition means an addition of single undersampled IFGs in that way, that each point, which is added refers to exactly the same optical path difference. The IFGs are aligned to the point of zero optical path difference (ZOPD). This is realized by assigning the peak position (POPD) of each IFG to the same optical path difference (OPD). This can be guaranteed only if the instrument is working in an absolutely stable mode, i.e. that no phase fluctuations occur, no misalignment, no effects of noise regarding the POPD (see figures in Subsection 6). To check for instrumental stability, the linear phase of each interferogram is calculated and compared. If the phase is not equal within a limited range, then the interferogram is discarded from co-adding.

For assigning time to the co-added IFGs the mean of the measuring times is used. The individual times of the IFGs are taken close to ZOPD. The same approach is taken for the localization, the line of sight (LOS) information and the blackbody temperature.

## Process flowchart



## Definitions of variables

Variable	Description	I/O	Type	Remarks
a	Number of interferograms to be co-added	I	i	default value := 1
$a_{\phi}^m$	offset of the linear phase of interferogram m	t	r	
$b_{\phi}^m$	slope of the linear phase of interferogram m	t	r	
A	number of co-added IFG's	O	i	initial value := 0
$b^m$	BB-temperature of single ifg <sup>m</sup>	I	r	
B	mean BB-temperature of co-added IFG	O	r	initial value := 0
c	type of derivation of the	I	o	possible values:

	POPD			<i>[maxpeak, nompeak, user defined]</i> default val. := maxpeak
$dx^m$	sampling interval of $ifg^m$	l	r	
$ifg_i^m$	point i within $ifg^m$	l	r	
$IFG_i$	point i within the co-added IFG	O	r	initial value :=0
m	index of the single Interferogram	t	i	range: [0..a-1]
$n^m$	number of points of $ifg^m$	l	i	
N	number of points of the co-added IFG	O	i	
$t^m$	time at ZOPD of single interferogram	l	d	
T	mean time at ZOPD of co-added IFG	O	d	initial value: greg2julian(T) := 0
$z^m$	point of POPD in $ifg^m$	t	i	range: [0.. $n^m$ -1]
Z	position of the POPD of the co-added IFG	O	i	
i	index variables	t	i	
j	number of points of the left side of the IFG	t	i	
k	number of points of the right side of the IFG	t	i	
$p^m$	nominal peak position of $ifg^m$	l	i	range [0.. $n^m$ -1]
$q^m$	user defined peak position of $ifg^m$	l	i	range [0.. $n^m$ -1]
$\varepsilon_a$	range in which the phase offset may vary	l	r	default value := $\pi/4$
$\varepsilon_b$	range in which the phase slope may vary	t	r	default value := $\frac{\pi}{4} / \frac{1}{2dx^m}$

## Algorithm

### Selection of IFG's

A selection of the IFGs to be co-added is done according to  $dx^m$ . Any  $ifg^m$  with  $dx^m$  not equal  $dx^1$  is discarded from co-adding.

### Determine POPD position

Depending of the value of  $c$ , the POPD position is identified as the position of the maximum positive value within the IFG or as the nominal peak position as defined by the optical setup and the hardware.

$$z^m = \begin{cases} \text{index\_of}(\max(\text{ifg}_i^m)) & \text{if } c = \text{maxpeak} \\ p^m & \text{if } c = \text{nompeak} \\ q^m & \text{if } c = \text{user defined} \end{cases}$$

### Check for instrumental stability

To check for instrumental stability, the linear phase of each interferogram (index  $m$ ) is calculated with the 'classical' phase determination and is compared to the phase of the first interferogram (index 0). If the difference of the offset  $a$  or slope  $b$  of the linear phase is larger than  $\epsilon_a$  respectively  $\epsilon_b$ , then the interferogram is discarded from co-adding. With the factor of  $1/\frac{1}{2dx^m}$  the criterion  $\epsilon_b$  for the slope the limitation is automatically aligned to the sampling distance. In the case that the true maximum is located in the middle between two sampling points, then the slope of the phase may switch between  $\pm\pi dx$ . To avoid this a default limit of the slope variation of  $\frac{\pi}{2} dx$  was chosen.

$$\text{co-addition, if } |a^0 - a^m| < \epsilon_a \quad \wedge \quad |b^0 - b^m| < \epsilon_b$$

### Co-addition

Performs the co-addition of the IFGs, shifted that way, that all POPD points will be on top of the other. This could lead to points at the far ends of the IFG to be co-added, for which no corresponding data point exist in the already co-added IFG. Therefore, the overall co-added IFG is limited to the largest common set of data points of all individual IFGs.

The normalisation of the co-added IFG is done during every co-addition step to allow a continuous visualisation of the co-addition process.

During every iteration of the co-addition process the mean temperature  $B$  of the blackbody and the mean measuring time  $T$  is calculated.

$$j = \begin{cases} z^m & \text{if } A = 0 \\ \min[Z, z^m] & \text{if } A > 0 \end{cases}$$

$$k = \begin{cases} n^m - z^m - 1 & \text{if } A = 0 \\ \min[N - Z - 1, n^m - z^m - 1] & \text{if } A > 0 \end{cases}$$

$$\text{IFG}_{j+i} = \frac{A \times \text{IFG}_{Z+i} + \text{ifg}^m z^{m+i}}{A+1} \quad \text{for } i = [-j, k]$$

$$T = \mathbf{julian\ 2\ greg} \left[ \frac{A \times \mathbf{greg\ 2\ julian}(T) + \mathbf{greg\ 2\ julian}(t^m)}{A+1} \right]$$

$$B = \frac{A \times B + b^m}{A+1}$$

$$Z = j$$

$$N = j + k + 1$$

$$A = A + 1$$

### Loop

A loop over all interferograms to be co-added is performed.

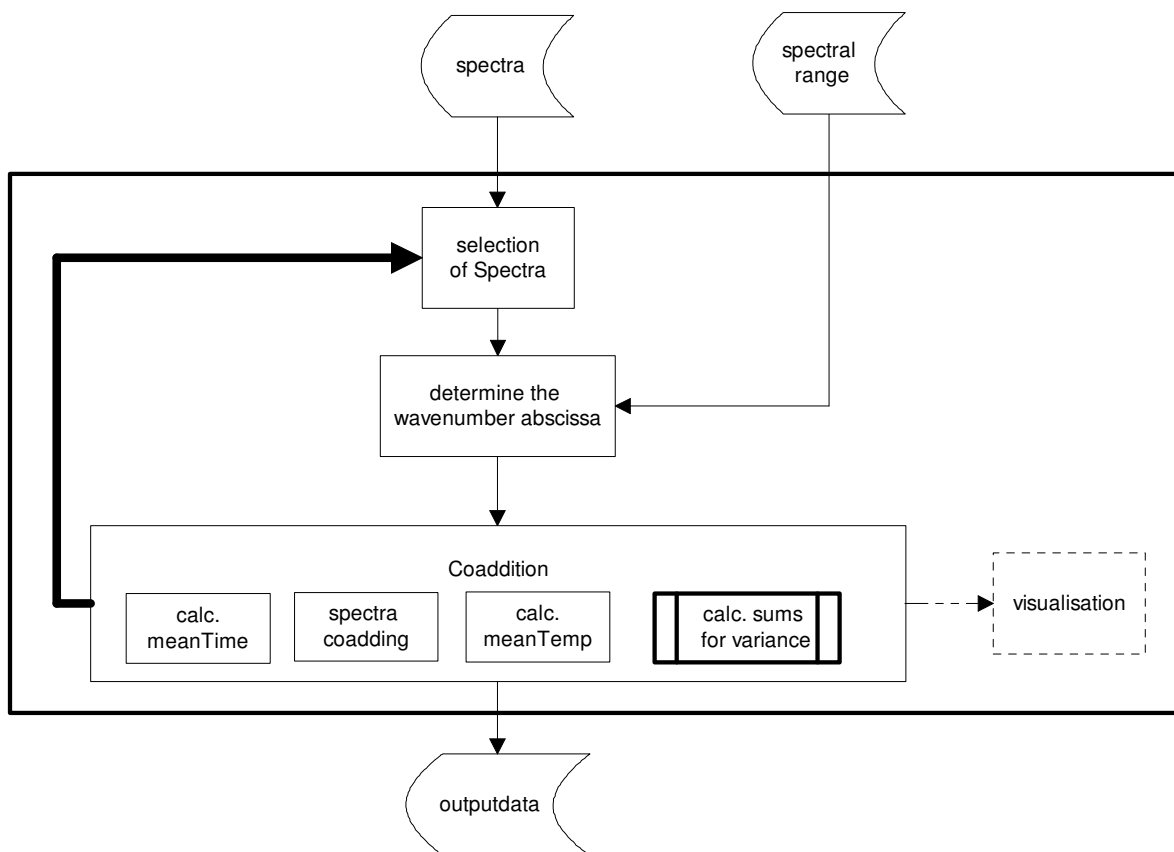
*From m=0 to a-1 do begin*  
*Selection of interferograms from the database*  
*Determination of POPD position*  
*Co-addition*  
*end*

### 8.3. Co-addition of spectra

#### Objective

Co-addition in the spectral domain is performed to reduce the noise in the spectra. It has the same functionality as the co-addition of the Interferograms, but usually the spectra are already based on phase corrected IFG's. Therefore the problem of phase instabilities doesn't have to be taken into account. The noise is reduced by a factor of  $A^{1/2}$  (A: number of co-added spectra). For co-addition in the spectral domain all spectra have to be on the same spectral grid, means that each point, which is added refers to an identical wavenumber.

#### Process flowchart



## Definitions of variables

Variable	Description	I/O	Type	Remarks
a	number of spectra to be co-added	l	i	defined by the number of selected spectra
A	number of co-added spectra	O	i	
$d\sigma^m$	wavenumber interval (spectral spacing) within $s^m$	l	r	defined by the first spectrum of the set of spectra to be co-added
$s_i^m$	point i within $s^m$	l	r	
$S_i$	point i within the co-added spectrum S	O	r	
m	index of s	t	i	
N	number of points of the co-added spectrum S	O	i	
$\sigma_L^m$	lowest wavenumber in $s^m$	t	r	
$\sigma_H^m$	highest wavenumber in $s^m$	t	r	
$\sigma_L$	lowest wavenumber in the co-added spectrum	t	r	
$\sigma_H$	highest wavenumber in the co-added spectrum	t	r	
i,j,k	index variables	t	i	
loop	loop variable	t		is <i>true</i> if spectra for co-adding are available

## Algorithm

### Selection of spectra

The spectra to be co-added need to have exactly the same spacing of the spectral points. A selection of the spectra to be co-added is done according to  $d\sigma^m$ . Any  $S^m$  with  $d\sigma^m$  not equal to  $d\sigma^1$  is discarded from co-adding.

### Determination of wavenumber abscissa

It is not absolutely necessary to have the same lower and higher bandwidth edges. Only common spectral points of the single spectra will be used for co-adding.

## Co-addition

Performs the co-addition of the spectra, shifted that way, that common spectral points will be on top of the other. This could lead to points at the far ends of the spectra to be co-added, for which no corresponding data point exist in the already co-added spectra. Therefore, the overall co-added spectrum is limited to the largest common set of spectral data points of all individual spectra.

The normalization of the co-added spectrum is done during every co-addition step to allow a continuous visualization of the co-addition process.

During every iteration of the co-addition process

- the mean temperature B of the blackbody
- and the mean measuring time T are calculated.
- The variance of the co-added spectra can iteratively determined within this step of co-adding.

$$\sigma_L = \max[\sigma_L, \sigma_L^m]$$

$$j = \text{indexof}(s, \sigma_L)$$

$$J = \text{indexof}(S, \sigma_L)$$

$$\sigma_H = \min[\sigma_H, \sigma_H^m]$$

$$k = \text{indexof}(s, \sigma_H)$$

$$S_i = \frac{A \times S_{J+i} + s_{j+i}^m}{A+1} \quad \text{for } i = [0 \dots k-j]$$

$$T = \text{julian 2 greg} \left[ \frac{A \times \text{greg 2 julian}(T) + \text{greg 2 julian}(t^m)}{A+1} \right]$$

$$B = \frac{A \times B + b^m}{A+1}$$

$$N = k - j + 1$$

$$A = A + 1$$

## Loop

A loop over all spectra to be co-added is performed.

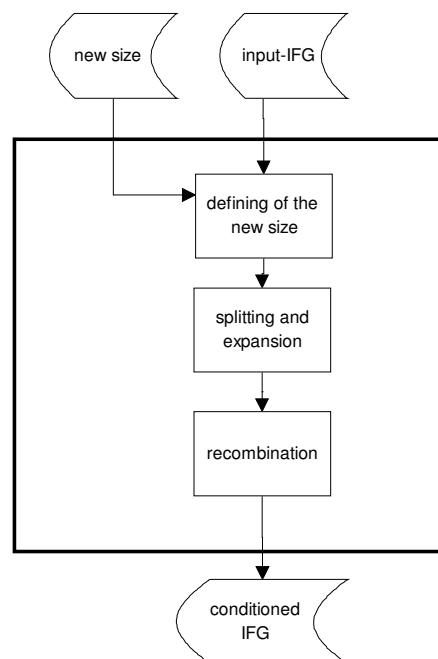
```
From m=0 to a-1 do begin
  Selection of spectra from the database
  Determine wavenumber abscissa
  Co-addition
end
```

## 8.4. Conditioning of data sets for FFT

### Objective

In contrast to real interferograms, which can have any size, the FFT algorithms need for best runtime performance input data with a number of points equal to a power of two. Additionally, the data points with negative OPD have to be shifted rightwards to the end of the dataset to achieve symmetry of the dataset for the FFT. The need originates in the discrete behaviour of the source data and can be best explained by the Nyquist theorem. This routine conditions the IFG to the above described constraints.

### Process flowchart



### Definitions of variables

Variable	Description	I/O	Type	Remarks
ifg	Original Interferogram	I	r	
IFG	Conditioned Interferogram	O	r	
n	number of data points in the IFG	I	i	

m	$\log_2$ of the size/2 of the output data	t	i	
s	max. output length of the conditioned IFG	I/O	i	default input value : s is not limited
$t^1$	right part of the IFG ( $x > 0$ )	t	r	
$t^2$	left part of the IFG ( $x < 0$ )	t	r	
z	point of POPD	l	i	

## Algorithm

### Definition of the new size

$$m = \log_2 \left[ \max[z, (n - z), (s / 2)] \right]$$

### Splitting and extension

$$t^1_{0..n-z-1} = \text{ifg}_{z..n-1}$$

$$t^1_{n-z..2^m-1} = 0$$

$$t^2_{2^m-z..2^m-1} = \text{ifg}_{0..z-1}$$

$$t^2_{0..2^m-z-1} = 0$$

### Recombination

$$\text{IFG}_{0..2^m-1} = t^1_{0..2^m-1}$$

$$\text{IFG}_{2^m..2^{m+1}-1} = t^2_{0..2^m-1}$$

## 8.5. Convolution of data sets using FFT

### Objective

The mathematical convolution of two functions can be performed by using the 'convolution theorem'.

$$g = f \otimes k = \mathbf{FFT}^{-1} \left[ \mathbf{FFT}^{+} [f] \mathbf{FFT}^{+} [k] \right]$$

If the number of points of the convolution kernel is larger than

$$\log_2(N), \quad N: \text{number of points of the function } f$$

a convolution by using FFT is appropriate to save computation time.

### Process flowchart

<none>

### Definitions of variables

Variable	Description	I/O	Type	Remarks
f	source function	I	r	
k	convolution kernel	I	r	
g	result	O	r	

### Algorithm

<library routine>

## 8.6. Fitting procedure with weighting coefficients

### Objective

This function performs a weighted least-squares polynomial fit by using matrix inversion. It is used to fit a polynomial to a one-dimensional vector by assigning the individual points of the vector with different weights.

This routine is a classical library function.

### Process flowchart

<none>

### Definitions of variables

Variable	Description	I/O	Type	Remarks
data	Input/output-data	I/O	r	
w	weighting parameter	l	r	w=0: no weighting w≠0: the power with which the weighting function is to be raised.
r	wavenumber range in which the fit has to be applied	l	r	default value is the overall spectral range of the input spectrum
o	the order of the polynom to be fitted	l	i	default value := 1 (linear function)
f	weighting function	l	r	Must have the same abscissa as the input - data

### Algorithm

<library routine>

## 8.7. Generation of spectra

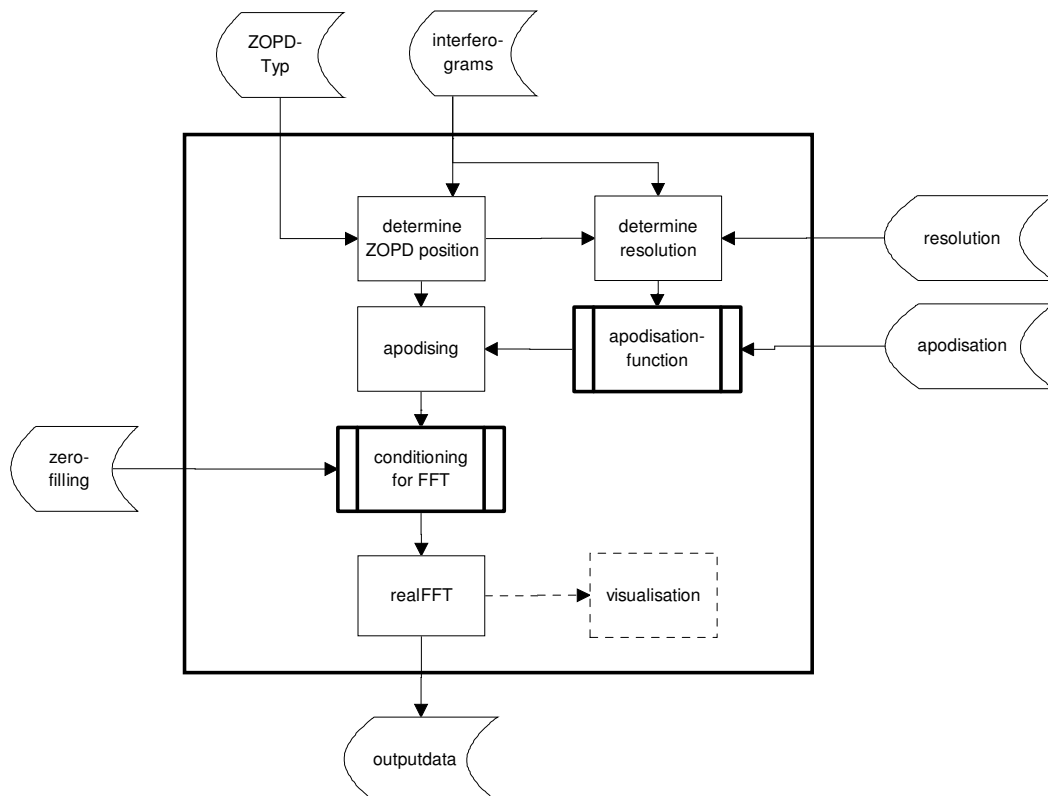
### Objective

The spectrum is derived by a real FFT from the corrected interferogram  $I_{(x)}$  which is degraded by the apodisation function  $A_{(x)}$ .

$$S_{(\sigma)} = \mathbf{FT}^+ [A_{(x)} I_{(x)}]$$

To interpolate between spectral points of the spectrum, the interferogram can be zero-filled after apodisation has been performed. Real FFT's are applicable on datasets with real values giving real symmetric and imaginary antisymmetric results. This a priori information allows to optimise the FFT process by nearly doubling the speed of the process and by allocating just the half of the memory space needed by a complex FFT. The symmetric counterparts of the real and imaginary spectrum are not returned by the real FFT.

### Process flowchart



## Definitions of variables

Variable	Description	I/O	Type	Remarks
apod	apodisation function	l	r	
c	type of derivation the POPD	l	o	Values: [ <i>maxpeak</i> , <i>nompeak</i> , <i>user defined</i> ] default val. := <i>maxpeak</i>
dx	sampling interval within ifg	l	r	
ifg <sub>i</sub>	point i within ifg	l	r	
IFG	apodised and conditioned IFG for FFT	O	r	
k	number of points of a single side of the IFG according to the selected resolution	t	i	
n	number of points of IFG <sup>m</sup>	l	i	
N	number of complex points in the spectrum	O	i	
p	nominal peak position of ifg <sup>m</sup>	t	i	range [0..n-1]
q	user defined peak position of ifg <sup>m</sup>	l	i	range [0..n-1]
γ	resolution	l	r	in cm <sup>-1</sup>
Γ	nominal resolution	O	r	in cm <sup>-1</sup>
z	point of selected POPD in IFG	t	i	Range: [0..n-1]
S	spectrum	O	c	
i,j,k	index variables	t	i	

## Algorithm

### Determine POPD position

Depending of the value of *c* the POPD position is identified as the position of the maximum positive value within the IFG or as the nominal peak position as defined by the optical setup and the hardware.

$$z = \begin{cases} \text{index\_of}(\max(\text{ifg}_i)) & \text{if } c = \text{maxpeak} \\ p & \text{if } c = \text{nompeak} \\ q & \text{if } c = \text{user defined} \end{cases}$$

### Determine resolution

The highest possible resolution is chosen, considering the constraints of the desired input value for the resolution and the length of the interferogram before and after the POPD.

$$\Gamma = \mathbf{max} \left[ \gamma, \frac{1}{2cdx}, \frac{1}{2(n-c-1)dx} \right]$$
$$k = \frac{1}{2\Gamma dx}$$

### Apodising

Performs the multiplication of the IFG with the apodisation function, shifted that way, that the symmetry point of the apodisation function will be shifted to the POPD of the IFG.

$$\text{IFG}_i = A_i \text{ifg}_{z-k+i} \quad \text{for } i = [0, 2k-1]$$

### Real-FFT:

As FFT a so called 'real FFT' is used, which has as input only a real input array. The result is a complex function with the real part transformed from the even part of the IFG and the imaginary part transformed from the odd part of the IFG.

The implementation is described in [Pres1986].

$$S = \mathbf{realfft}(\text{IFG})$$

## 8.8. Generation of the variance of single consecutive spectra

### Objective

The variance is used to determine the impact of statistical noise onto the co-added spectrum.

$$v_i = \frac{\sum_{n=1}^N (S_{i,n} - \bar{S}_i)^2}{N-1}$$

For memory reasons it is advantageous to obtain the variance iteratively with each step of co-addition of the calibrated spectra.

The equation to determine the variance can be rewritten with

$$v_i = \frac{\sum_{n=1}^N S_{i,n}^2 - \left( \sum_{n=1}^N S_{i,n} \right)^2 / N}{N-1} .$$

The two sums and in the equation above can be added separately at each iteration step.

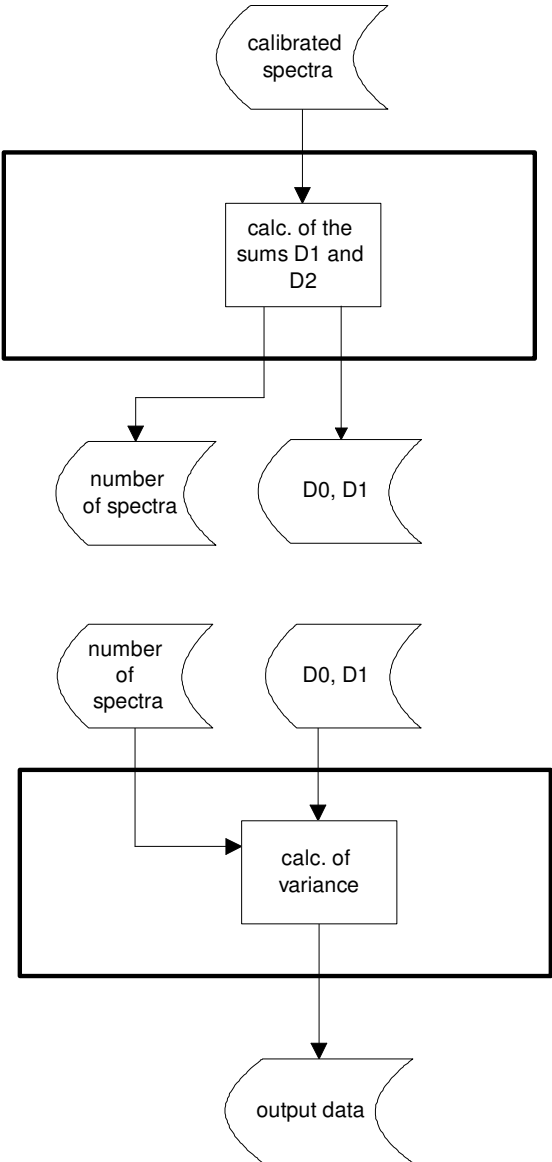
$$D0 = \sum_{n=1}^N S_{i,n}$$

$$D1 = \sum_{n=1}^N S_{i,n}^2$$

The variance is then calculated at the end of the iteration by

$$v_i = \frac{D1 - D0^2 / N}{N-1}$$

Process flowchart



## Definitions of variables

Variable	Description	I/O	Type	Remarks
S	Individual spectrum of the co-added spectrum	l	r	
i	point within single spectrum, element of the matrix	t	i	
n	indices of the spectrum	t	i	Range: 1..N
v	covariance matrix	O	r	
D0	sum	t/l	r	
D1	sum of squares	t/l	r	
N	number of spectra	l	i	defined by the number of selected spectra

## Algorithm

### Calculation of the sums D0 and D1

This process can be started on each calibration process. It has to be validated that all calibrated spectra have the same wavenumber axis. The calculation of the sums is normally performed during co-addition of the calibrated spectra (Subsection 8.3), but can also be performed separately.

$$D0 = \sum_{n=1}^N S_{i,n}$$

$$D1 = \sum_{n=1}^N S_{i,n}^2$$

### Calculation of the variance

The variance is then calculated at the end of the iteration over all calibrated spectra by

$$v_i = \frac{D1 - D0^2/N}{N - 1}$$

## 8.9. Interferogram correction and mathematical filtering

### Objective

The phase disturbed IFG is corrected such that the desired spectrum is purely real and any beamsplitter contributions are purely imaginary. Within this process the bandwidth of the spectrum can be limited by a mathematical band-pass filter  $b(\sigma)$ .

$$\begin{aligned}
 S_{\text{corr}(\sigma)} &= S_{(\sigma)} e^{i\Phi(\sigma)} b_{(\sigma)} \\
 \mathbf{FT}[\text{IFG}_{\text{corr}(x)}] &= \mathbf{FT}[\text{ifg}_{(x)}] e^{i\Phi(\sigma)} b_{(\sigma)} \\
 &= \mathbf{FT}[\text{ifg}_{(x)} \otimes \mathbf{FT}[e^{i\Phi(\sigma)} b_{(\sigma)}]] \\
 &\Rightarrow \\
 \text{IFG}_{\text{corr}(x)} &= \text{ifg}_{(x)} \otimes \underbrace{\mathbf{FT}[e^{i\Phi(\sigma)} b_{(\sigma)}]}_{k_{(x)}^*}
 \end{aligned}$$

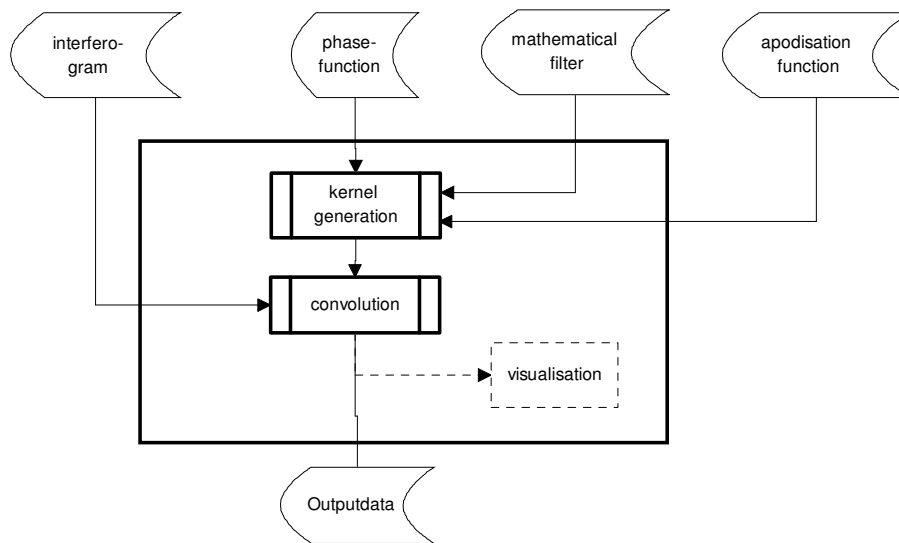
The resulting kernel  $l(x)$  is optimised by the tapering function  $A(x)$  to reduce the wiggles of the Gibb's phenomena. The tapering function can be any apodisation function.

$$k_{(x)} = k_{(x)}^* A_{(x)}$$

The corrected IFG is performed by a convolution of the disturbed IFG with the kernel  $k(x)$ .

$$\text{IFG}_{\text{corr}(x)} = \text{ifg}_{(x)} \otimes k_{(x)}$$

## Process flowchart



## Definitions of variables

Variable	Description	I/O	Type	Remarks
m	index	t	i	
b	Mathematical band-pass-filter	l	r	default is no bandpass limitation
$\Phi$	phase function	l	r	
ifg	Input interferogram	l	r	
apod	Tapering-function	l		possible values: [NS, NM, NW, FD, FE, RE, TA, TR] default value := NS
IFG	Corrected Interferogram	O	r	
k	kernel function	t	r	

## Algorithm

The routine uses no specific algorithm. See Subsection 8.10 and 8.5 for kernel generation and convolution

## 8.10. Kernel generation

### Objective

For phase correction of interferograms a convolution kernel is needed:

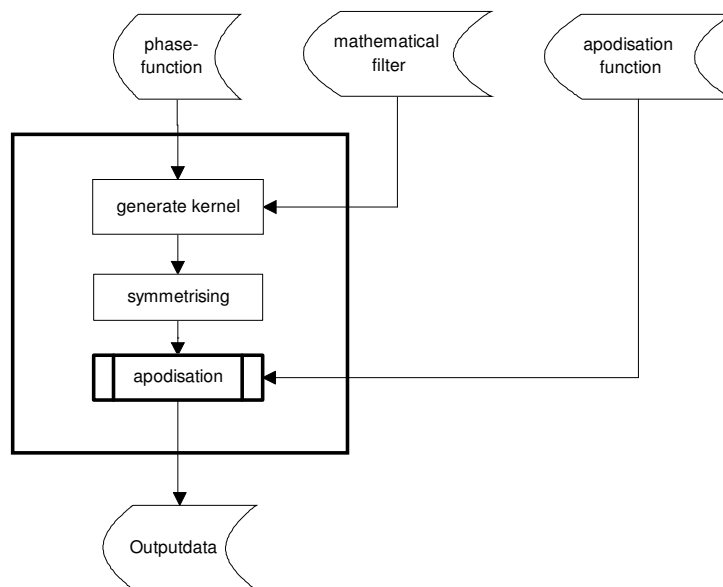
The phase disturbed IFG is corrected by a given phase  $\Phi(\sigma)$ . During this process the spectrum can be limited by a mathematical band-pass filter  $b(\sigma)$ . Both parameters are given in the spectral domain which are to be transformed into the space domain.

$$k_{(x)}^* = \text{FT}[e^{i\Phi(\sigma)} b_{(\sigma)}]$$

The resulting kernel  $k(x)$  is optimized by the tapering function  $A(x)$  to reduce the wiggles of the Gibb's phenomena. The tapering function can be any apodisation function.

$$k_{(x)} = k_{(x)}^* A_{(x)}$$

### Process flowchart



## Definitions of variables

Variable	Description	I/O	Type	Remarks
m	index	t	i	
b	bandpassfilter	l		default is no bandpass limitation
$\Phi$	phase function	l		
t	temporary vector	t		
$k^*$	non-apodised kernel	t		
N	number of points of the phase function	l		
k	kernel function	O		

## Algorithm

### Generating the kernel

The bandwidth filtering vector  $b$  is adjusted to have the same abscissa as the phase function  $\Phi$ , which again must have the same abscissa as the Fourier transformed of interferogram which is to be phase-corrected.

$$t_m = e^{i\Phi_m} b_m$$

$$t = \text{FFT}(t)$$

### Symmetrising

The correction function has to be symmetrised around the center point at  $N/2$  of the vector  $t$ :

$$k_{N/2 \dots N-1}^* = t_{0 \dots N/2-1}$$

$$k_{0 \dots N/2-1}^* = t_{N/2 \dots N-1}$$

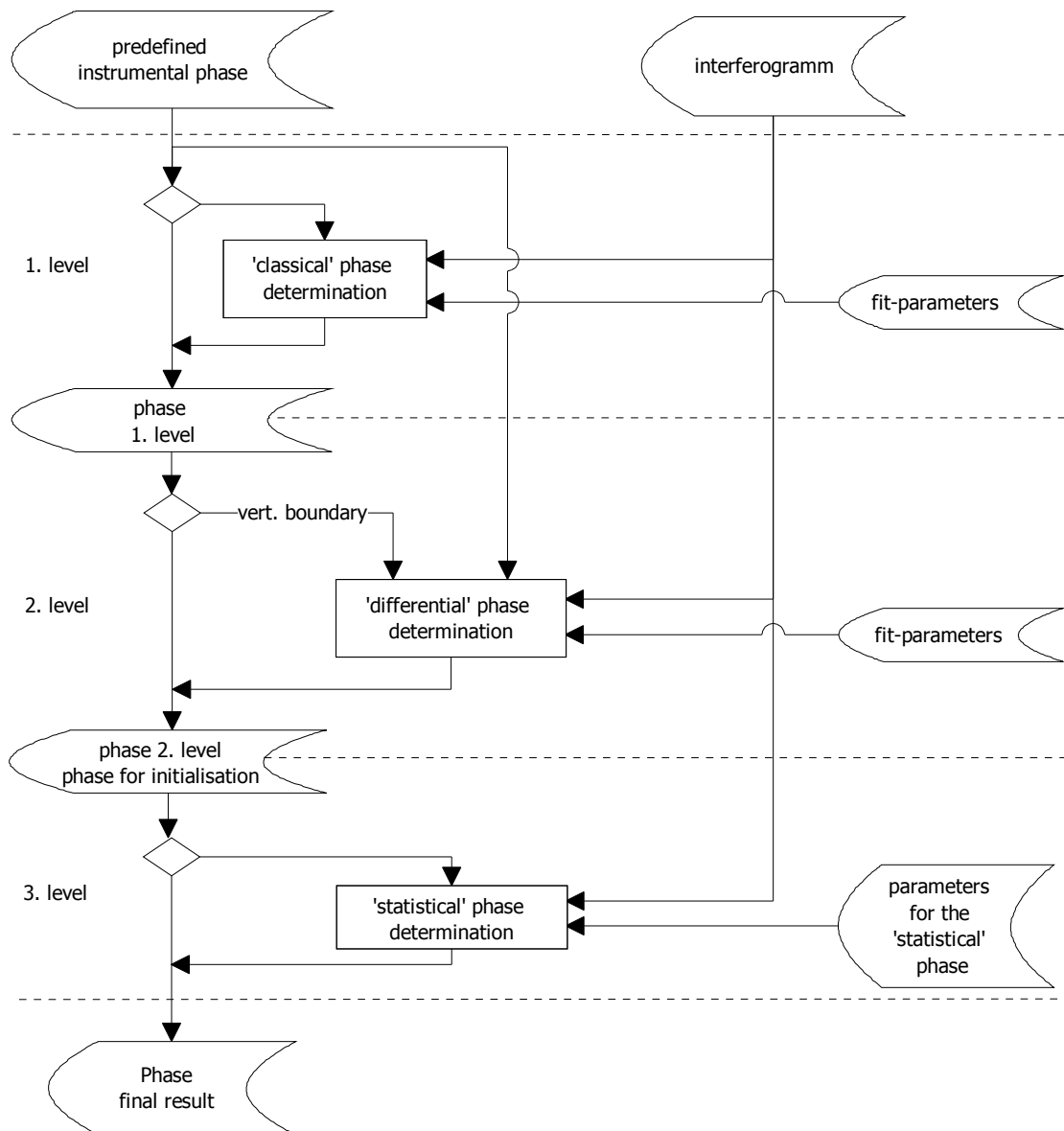
The final kernel function  $k$  is apodised to reduce the wiggles in the spectrum due to the band-pass filter.

## 8.11. Phase determination

### Objective

<as described in chapter 6.2>

### Process flowchart



### 8.11.1. 'Classical' phase determination

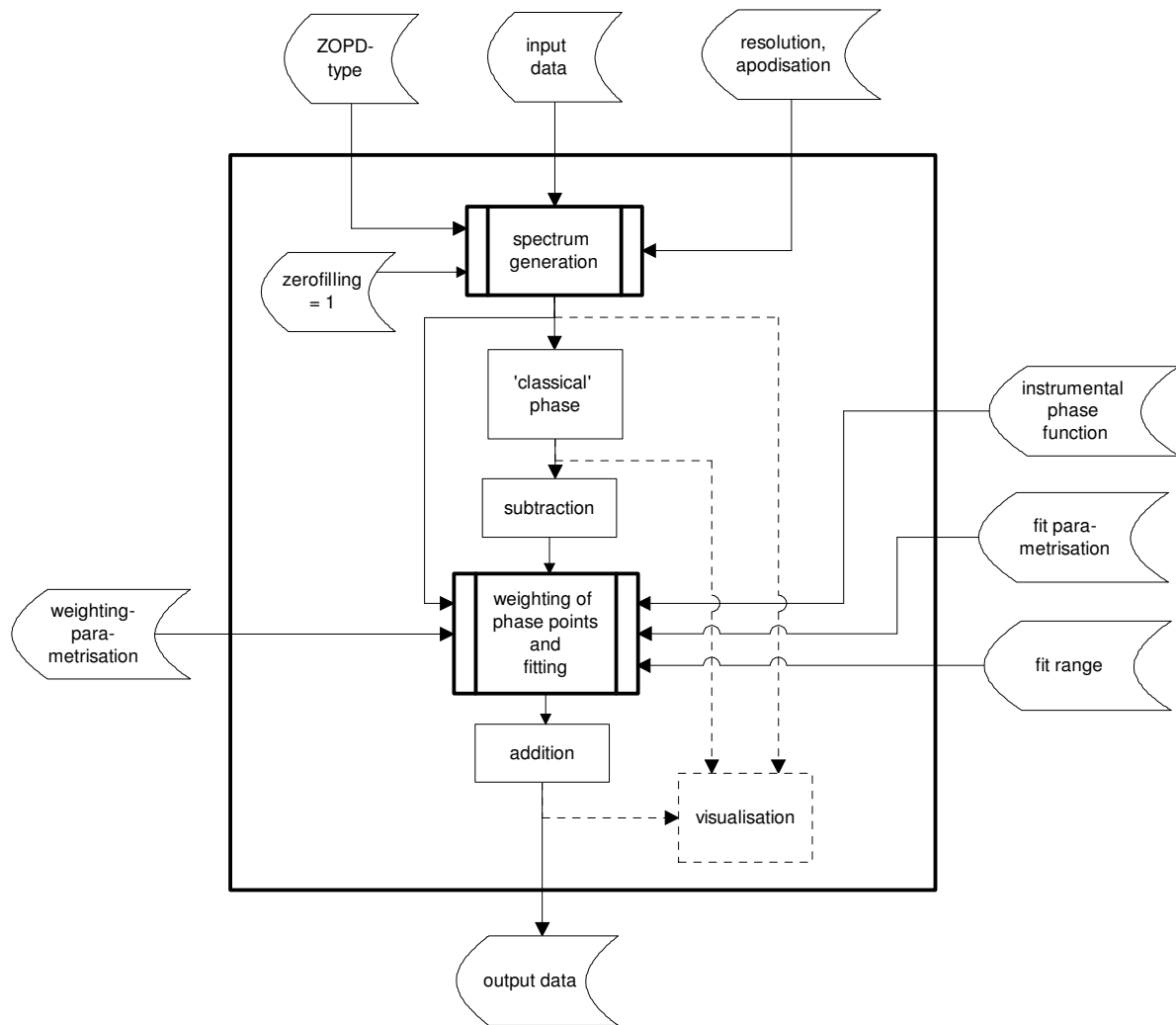
#### Objective

The phase is obtained by the angle between the real and imaginary part of the complex spectrum  $S_{(\sigma)}$  (classical approach by [Form1966]). The spectrum is derived by a FFT from the interferogram  $I_{(x)}$  which is degraded by the apodisation function  $A_{(x)}$ .

$$S_{(\sigma)} = \text{FT}^+ \left[ A_{(x)} I_{(x)} \right]$$
$$\phi_{c(\sigma)} = \arctan \left[ \frac{\text{Im} \left[ S_{(x)} \right]}{\text{Re} \left[ S_{(x)} \right]} \right]$$

The noise in the spectrum is propagated to the phase function which should be a smooth and noiseless function. Therefore the phase function is fitted with a well defined instrumental phase, derived from a black-body measurement. Only linear phase shifts could be reasonably determined, so that a first order linear square fit is performed. At spectral points where the interferometer ports are well balanced, the phase is ill defined. This appears mostly at low spectral radiances of the scene. Therefore, to reduce these effects, the phase points to be fitted are weighted by the square of the absolute spectral intensity.

## Process flowchart



## Definitions of variables

Variable	Description	I/O	Type	Remarks
apod	apodisation function type	l	r	Values: [NS, NM, NW, FD, FE, RE, TA, TR] default value := NS
c	type of derivation of the POPD	l	o	possible values: [maxpeak, nompeak, user defined] default val. := maxpeak
dx	sampling interval within ifg	l	r	
i	index variables	t	i	range: [0..m-1]

ifg <sub>i</sub>	point i within ifg	l	r	
m	number of complex points in spectrum S	t	i	
n	number of points of IFG <sup>m</sup>	l	i	
o	the order of the polynom to be fitted	l	i	range: [0..5] default: Linear function
r	wavenumber range in which the fit has to be applied	l	r	see subsection 7
S <sub>i</sub>	point i of complex spectrum S	t	c	
w	weighting parameter	l	r	default value := 2
Z	zerofilling	t	i	Z=1, means no zerofilling is used
Φ <sub>i</sub>	point i within the phase function Φ	O,t	r	
γ	resolution	l	r	default is the max. resolution defined by the length of the IFG

## Algorithm

### Classical phase

The arc-tangent function returns the phase angle of the complex spectrum, expressed in radians. The range of the phase is between  $-\pi$  and  $\pi$ .

$$\phi_i = \arctan[\operatorname{Re}(S_i), \operatorname{Im}(S_i)] \quad \text{with} \quad \phi_i \in [-\pi, \pi]$$

$$i = [0..m-1]$$

## 8.11.2. Differential Phase determination

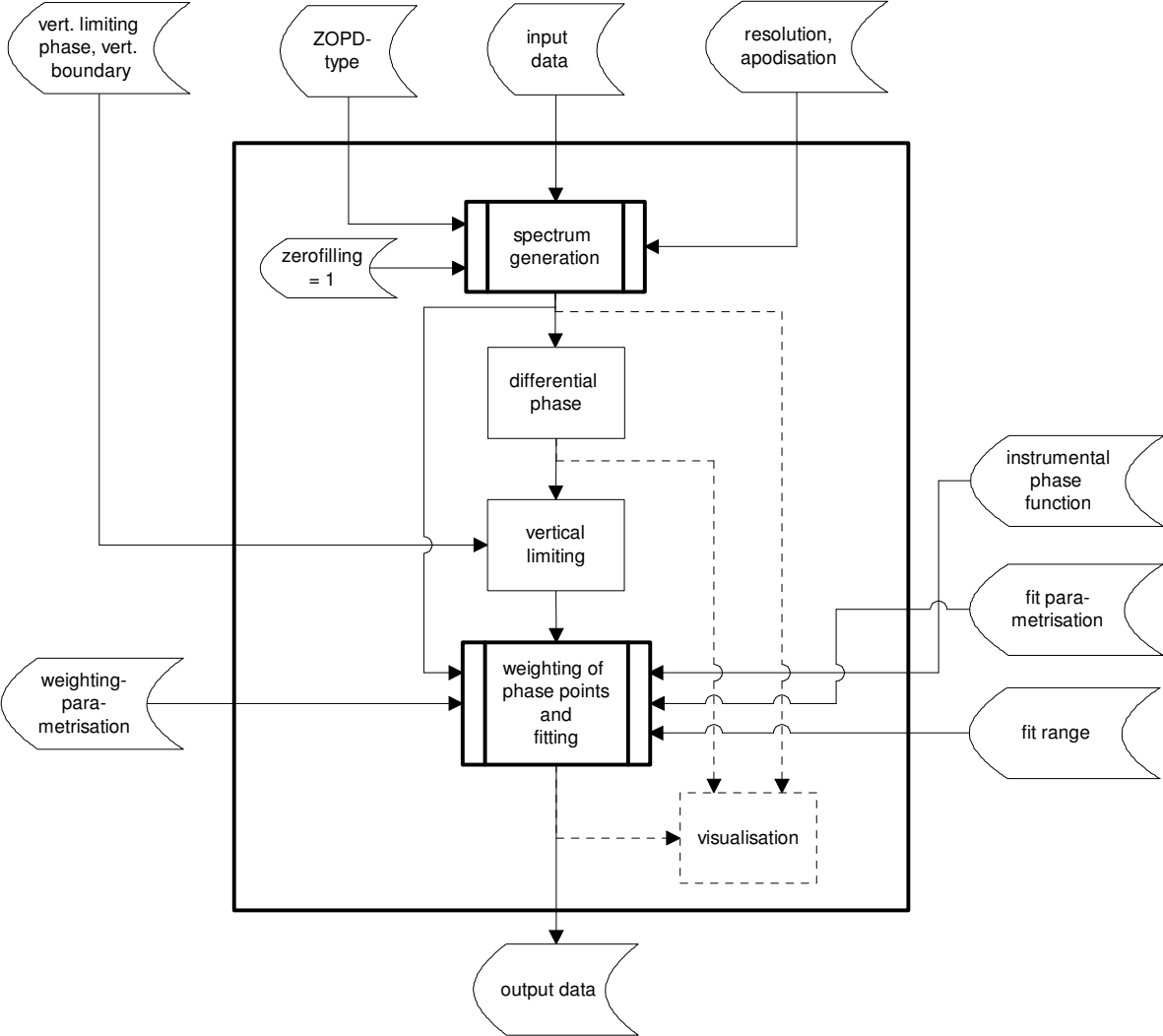
### Objective

The 'differential' phase [Wedd1993] is defined as the angle between the derivatives of the imaginary and real part of the complex spectrum. The spectrum to be determined is derived by a complex FFT of the interferogram  $I_{(x)}$  which is degraded by the apodisation function  $A_{(x)}$ .

$$S_{(\sigma)} = \text{FT}^+(A_{(x)}I_{(x)})$$
$$\Phi_{d(\sigma)} = \arctan \left[ \frac{\text{Im} \left( \frac{\partial S_{(\sigma)}}{\partial \sigma} \right)}{\text{Re} \left( \frac{\partial S_{(\sigma)}}{\partial \sigma} \right)} \right]$$

The differential phase is fitted the same way as described in the paragraph of the 'classical' phase approach.

**Process flowchart**



## Definitions of variables

Variable	Description	I/O	Type	Remarks
apod	apodisation function type	l	r	Values: [NS, NM, NW, FD, FE, RE, TA, TR] default value := NS
c	type of derivation of the POPD	l	o	Values: [maxpeak, nompeak, user defined] default val. := maxpeak
dx	sampling interval within ifg	l	r	
i	index variables	t	i	range: [0..m-1]
ifg <sub>i</sub>	point i within ifg	l	r	
m	number of complex points in spectrum S	t	i	
n	number of points of IFG <sup>m</sup>	l	i	
o	the order of the polynom to be fitted	l	i	range: [0..5] default: linear function
r	wavenumber range in which the fit has to be applied	l	r	see subsection 7
S <sub>i</sub>	point i of complex spectrum S	t	c	
S' <sub>i</sub>	Derivative of S	t	c	
w	weighting parameter	l	r	default val. := 2
Z	zerofilling	t	i	Z=1, means no zerofilling is used
Φ <sub>i</sub> <sup>*</sup>	point i within the phase function Φ <sup>*</sup> obtained from the derivative	t	r	Range: [-π/2 .. π/2]
Φ <sub>S,i</sub>	point i within the initial phase function Φ <sub>S</sub>	l,t	r	
Φ <sub>i</sub>	point i within the differential phase function Φ	O,t	r	
γ	resolution	l	r	default is the max. resolution defined by the length of the IFG

## Algorithm

### Differential phase

The arc-tangent function returns the phase angle of the derivated complex spectrum, expressed in radians. The range of the phase is between  $-\pi/2$  and  $\pi/2$ .

$$S'_i = \frac{S_{i+1} - S_{i-1}}{2dx}$$

$$\Phi_i^* = \arctan[\text{Im}(S'_i)/\text{Re}(S'_i)]$$

with

$$\Phi_i^* \in [-\pi/2, \pi/2]$$

$$i = [1..m - 2]$$

### Vertical limiting

Since the arctan is repetitive with  $\pi$ , therefore the phase may jump about  $\pi$ , when the real part of the derivative is changing sign. To reduce this effect a vertical boundary band is introduced which is defined by the initial phase  $\pm\pi/2$ .

$$\Phi_i = \arctan\left[\tan\left[\Phi_i^* - \Phi_{S,i}\right]\right] + \Phi_{S,i}$$

### 8.11.3. Statistical phase determination

#### Objective

Noise in the differential spectra may deteriorate the accuracy of the differential phase, especially in case of single non-co-added spectra. This affects the accuracy of the phase corrected spectrum to an unacceptable level.

The quality of the phase retrieval can be enhanced by applying some a-priori constraints:

- As already explained, the total phase-function can be separated into a instrumental part  $\Phi^*_{(\sigma)}$  and a linear part  $\Delta\Phi_{(\sigma)}$ . The second one can be expressed as a straight line with the parameters offset  $a$  and slope  $b$ .

$$\Phi_{(\sigma)} = \Phi^*_{(\sigma)} + \Delta\Phi_{(\sigma)} = \Phi_{(\sigma)} + a + b(\sigma - \sigma_0)$$

- the correlation between the atmospheric and the beamsplitter spectrum has to vanish:

$$\mu = \text{correl}(\text{Re}(S), \text{Im}(S)) \rightarrow \pm 0$$

To avoid the correlation between the imaginary and real part of the spectra with respect to the spectral response (due to the Planck- and filter-function), each part is highpass filtered.

- the variance of the beamsplitter spectrum has to be minimised. For better convergence the elements of the variance are squared:

$$\begin{aligned} \frac{d(v^2)}{d(\Delta\Phi)} &= \frac{d \text{variance}(\text{Im}^2(S))}{d(\Delta\Phi)} = 0 \\ &= \frac{d \sum_i [\text{Im}(S_{\Phi^*,i}) + \text{Re}(S_{\Phi^*,i})\Delta\Phi]^4}{d(\Delta\Phi)} \end{aligned}$$

A solution is found, if:

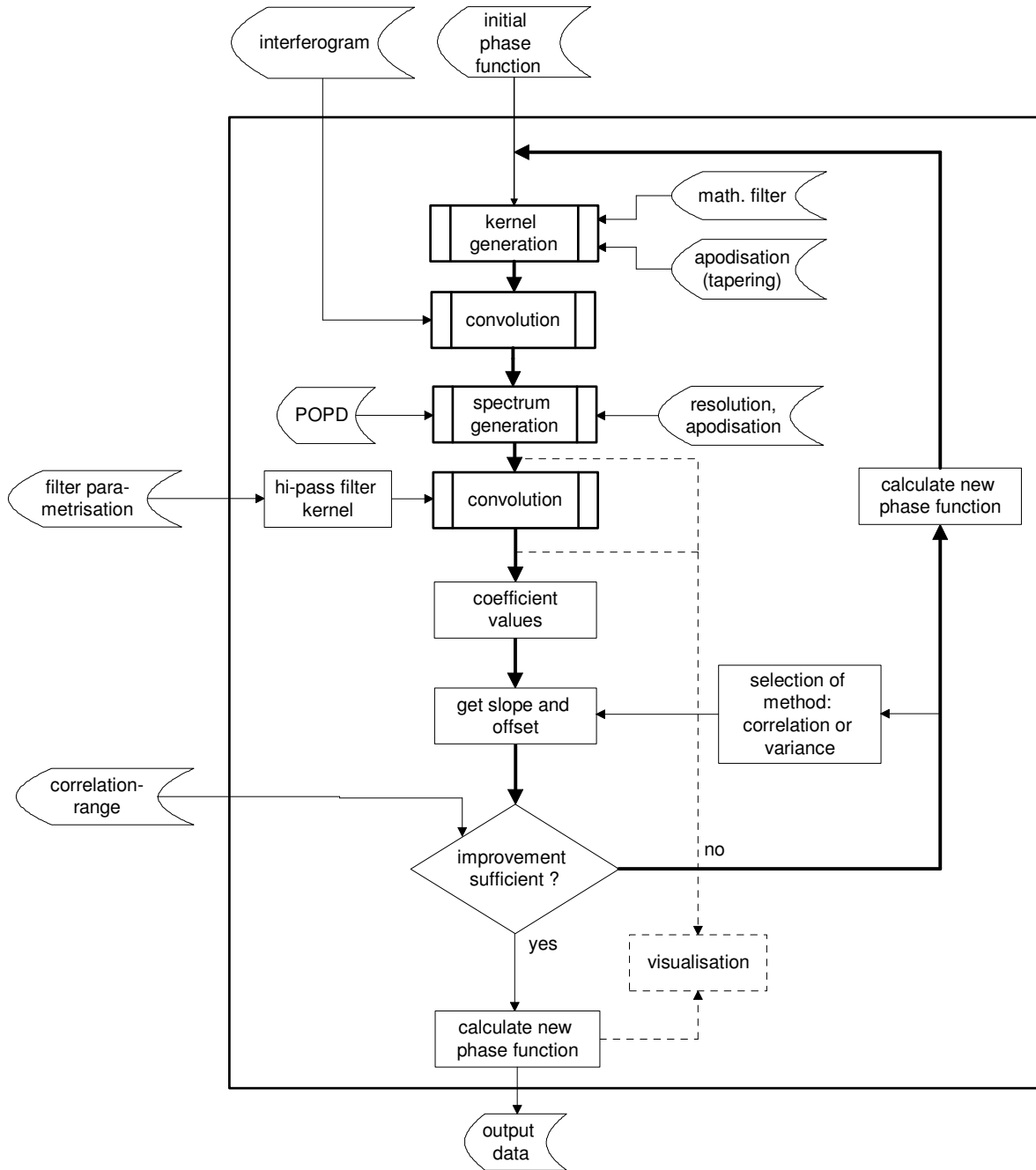
$$\begin{aligned} \frac{\partial(v^2)}{\partial a} &= 0 \\ \frac{\partial(v^2)}{\partial b} &= 0 \end{aligned}$$

The correlation  $\mu$  converges rapidly for the phase-offset  $a$ . But for the slope  $b$  the positive line correlations of one side of the spectral band may be compensated by negative line correlations of the other side. On the other hand  $v$  does not converge rapidly for the offset  $a$  but for the slope  $b$ . A combination at each iteration step of  $\mu$  for the offset and of  $v$  for the slope  $b$  results in a good convergence for both parameters.

The complex spectrum used in all steps of this phase determination method is derived by a classical real FFT from the interferogram  $I(x)$  which is degraded by the apodisation function  $A(x)$ .

$$S_{(\sigma)} = \text{FT}^+ [A(x) I(x)]$$

**Process flowchart**



## Definitions of variables

Variable	Description	I/O	Type	Remarks
a	offset	t	r	
b	slope	t	r	
$c_i$	coefficients for variance and correlation	t	r	
$f_l$	lower frequency of the filter in fractions of the Nyquist frequency	l	r	default value := 0.4
gibb	reduction of the gibb' phenomena	l	r	expressed in dB
$k_i$	kernel function	t	r	
order	order of the kernel	l	i	default value := 100
m	index	t	i	
result		t	b	
step	iteration	t	i	initial value: step=0
$step_{limit}$	limit of iteration steps	l	r	default value := 15
$z_i$	operator variable	t	r	
$\alpha$	Bessel coefficient	t	r	
$\epsilon_v$	limit of the variance change from step to step	l	r	default value := 2e-4
$\epsilon_\mu$	limit of the correlation change from step to step	l	r	default value := 2e-4
$\epsilon_\phi$	limit of the phase uncertainty	l	r	default value := 20mrad
$\Phi_i^*$	instrumental phase function	l	r	
$\Phi_i$	corrected phase function	O	r	
$\mu$	correlation coefficient	t,O	R	
$\nu$	variance coefficient	t,O	R	
$\sigma_i$	wavenumber at point i	l	r	
$\sigma_L$	low wavenumber of bandwidth interval	l	r	see section 7
$\sigma_H$	high wavenumber of bandwidth interval	l	r	see section 7
$\sigma_0$	medium wavenumber of bandwidth interval	t	r	

## Algorithm

### High pass filter kernel

The digital filtering is performed by convolution of the spectrum with a kernel function representing the hi-pass filter.

The kernel returns the coefficients of a non-recursive, digital filter for evenly spaced data points. The kernel coefficients are Kaiser-weighted. The intensity of the Gibbs phenomenon wiggles can be defined in -db; a suppression value of -50db is appropriate. Frequencies are expressed in terms of the Nyquist frequency,  $1/dx/2$ , where  $dx$  is the interval between data samples. The resulting vector of coefficients has  $(2 \times \text{order} + 1)$  elements.

$$\alpha = \begin{cases} 0 & \text{for } \text{gibb} \leq 21 \\ 0.5842(\text{gibb} - 21.)^{0.4} + 0.07886(\text{gibb} - 21.) & \text{for } 21 < \text{gibb} < 50 \\ 0.1102(\text{gibb} - 8.7) & \text{for } \text{gibb} \geq 50 \end{cases}$$

$$k_{m+\text{order}} = \frac{\sin(-i\pi f_1)}{i\pi} \frac{\mathbf{I}\left(\alpha \sqrt{1 - \left(\frac{m}{\text{order}}\right)^2}, 0\right)}{\mathbf{I}(\alpha, 0)} \quad m = [1..\text{order}]$$

$$k_{\text{order}} = 1 - f_1$$

$$k_{m-1} = k_{2 \times \text{order} - m + 1}$$

with  $\mathbf{I}(\alpha, x)$ : Besselfunction

### Coefficient values

The coefficient values can be directly derived from the high-pass filtered spectra.

For the next equations the following operator will be used to take the spectral

$$\text{Operator } O\langle z_m \rangle = \sum_m \begin{cases} 0 & \text{if } \sigma_m < \sigma_L \\ 0 & \text{if } \sigma_m > \sigma_H \\ z_m & \text{else} \end{cases}$$

bandwidth into account.

The use of the mean wavenumber of the spectral bandwidth is appropriate to increase the numerical accuracy:

The coefficients are given by:

$$\begin{aligned}
 c_1 &= O\langle \mathbf{Re}(S_m) \mathbf{Im}(S_m) \rangle \\
 c_2 &= O\langle \mathbf{Re}(S_m)^2 - \mathbf{Im}(S_m)^2 \rangle \\
 c_3 &= O\langle 4 \mathbf{Re}(S_m) \mathbf{Im}(S_m)^3 \rangle \\
 c_4 &= O\langle 4(\sigma_m - \sigma_0) \mathbf{Re}(S_m) \mathbf{Im}(S_m)^3 \rangle \\
 c_5 &= O\langle 12 \mathbf{Re}(S_m)^2 \mathbf{Im}(S_m)^2 \rangle \\
 c_6 &= O\langle 12(\sigma_m - \sigma_0) \mathbf{Re}(S_m)^2 \mathbf{Im}(S_m)^2 \rangle \\
 c_7 &= O\langle 12(\sigma_m - \sigma_0)^2 \mathbf{Re}(S_m)^2 \mathbf{Im}(S_m)^2 \rangle
 \end{aligned}$$

$$\sigma_0 = \frac{O\langle \sigma_m \rangle}{O\langle 1 \rangle} \quad m = [0..n-1]$$

### Get slope and offset

correlation method: 
$$a = \min \left[ \frac{1}{2} \frac{c_2}{c_1} \mp \sqrt{1 + \left( \frac{1}{2} \frac{c_2}{c_1} \right)^2} \right]$$

variance method: 
$$\begin{aligned}
 a &= \frac{c_3 c_7 - c_4 c_6}{c_6^2 - c_5 c_7} \\
 b &= \frac{c_4 c_5 - c_3 c_6}{c_6^2 - c_5 c_7}
 \end{aligned}$$

### Get phase-function

$$\Phi_m = \Phi_m^* + a + b(\sigma_m - \sigma_0)$$

## Loop criterion

Stop of variance minimisation:

$$\text{result} = (v_{\text{step-1}} - v_{\text{step}}) < \varepsilon_v$$

Stop of correlation minimisation:

$$\text{result} = |\mu_{\text{step-1}} - \mu_{\text{step}}| < \varepsilon_\mu$$

correlation coefficient low:

$$\text{result} = \Phi_{\text{uncertainty}} < \varepsilon_\Phi$$

Stop of iteration because of limited steps:

$$\text{result} = \text{step} > \text{step}_{\text{limit}}$$

with

$$\text{result} \in [\text{true}, \text{false}]$$

## 8.12. Radiometric calibration of the spectra

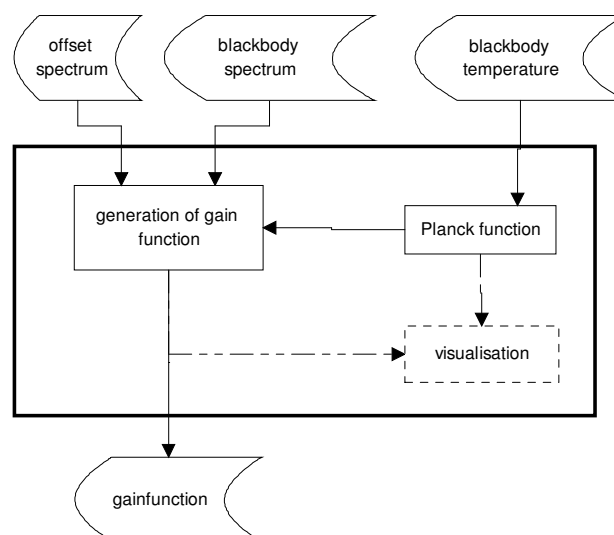
### Objective

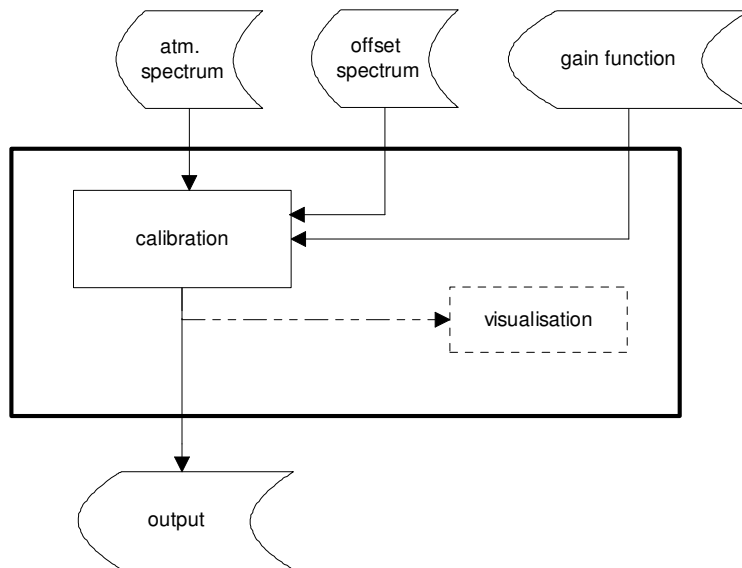
The radiometric calibration allows to convert the uncalibrated values into physical units of spectral radiance. A two point calibration is performed. One calibration “point” is derived from the instrumental self emission spectrum which is determined from ‘shaved’ deep-space spectra. This spectrum is subtracted from the uncalibrated one. The other calibration “point” is a spectrum of a relatively ‘hot’ blackbody (~210K). Together with the corresponding Planck-function, which acts as an ideal spectrum for the blackbody, a gain function is derived:

$$S_{\text{calib}} = (S_{\text{atm.}} - S_{\text{offset}}) \underbrace{\left[ \frac{S_{\text{BB}} - S_{\text{offset}}}{S_{\text{Planck}}} \right]^{-1}}_{\text{Gainfunction}}$$

The calibration is performed by subtraction of the instrumental self-emission spectrum from the atmospheric spectrum and afterwards multiplying with the gain function.

### Process flowchart





### Definitions of variables

Variable	Description	I/O	Type	Remarks
$S_{atm}$	Atmospheric spectrum	l	r	
$S_{offset}$	Offset, instrumental background (self emission) spectrum	l	r	
$S_{BB}$	Blackbody spectrum	l	r	
$S_{Planck}$	Planck function	l	r	
$g$	Gain-function	I/O	r	
$T$	Blackbody temperature	l	r	
$\sigma_i$	Wavenumber at index i	t	r	
$S_{calib}$	Calibrated spectrum	O	r	

### Algorithm

#### Planck function

$$S_{Planck,i} = \frac{2hc^2 \sigma_i^3 * 10^{-14}}{e^{\frac{hc}{10kT} * \sigma_i} - 1}$$

with

$$h = 6.626176$$

$$c = 2.99792$$

$$k = 1.38062$$

### Generation of gain function

The gain-function  $g$  can be used for calibrating several spectra. Therefore the gain-function is calculated separately and is stored for reuse. The abscissa (the wavenumber scale) of the deep-space spectrum  $S_{\text{offset}}$  has to be aligned to the blackbody spectrum.

$$g_i = \frac{S_{\text{Planck},i}}{(S_{\text{BB},i} - S_{\text{offset},i})}$$

### Calibration

The abscissa of the deep-space spectrum  $S_{\text{offset}}$  and the gain-function  $g_i$  have to be aligned to the atmospheric spectrum.

$$S_{\text{calib},i} = (S_{\text{atm},i} - S_{\text{offset},i}) g_i$$

## 8.13. 'Shaving' - Removal of residual atmospheric lines in deep space spectra

### Objective

The 'shaving' of spectra is necessary to remove any sharp spectral lines from the deep space spectra. To be independent of spectral databases and to be as selective as possible, the individual lines in the spectra have been identified and removed separately.

Task one in the removal process is to distinguish between lines which have to be removed, and broadband features which have to remain in the offset spectrum. High altitude spectral lines are sharp and almost purely in the Doppler-broadening regime in the IR. They have a relatively strong gradient at the line wings and a strong curvature at their peaks. The selection of those lines was performed by finding high absolute values of the geometric sum  $S^d$  of the first and second derivative of the spectral intensity.

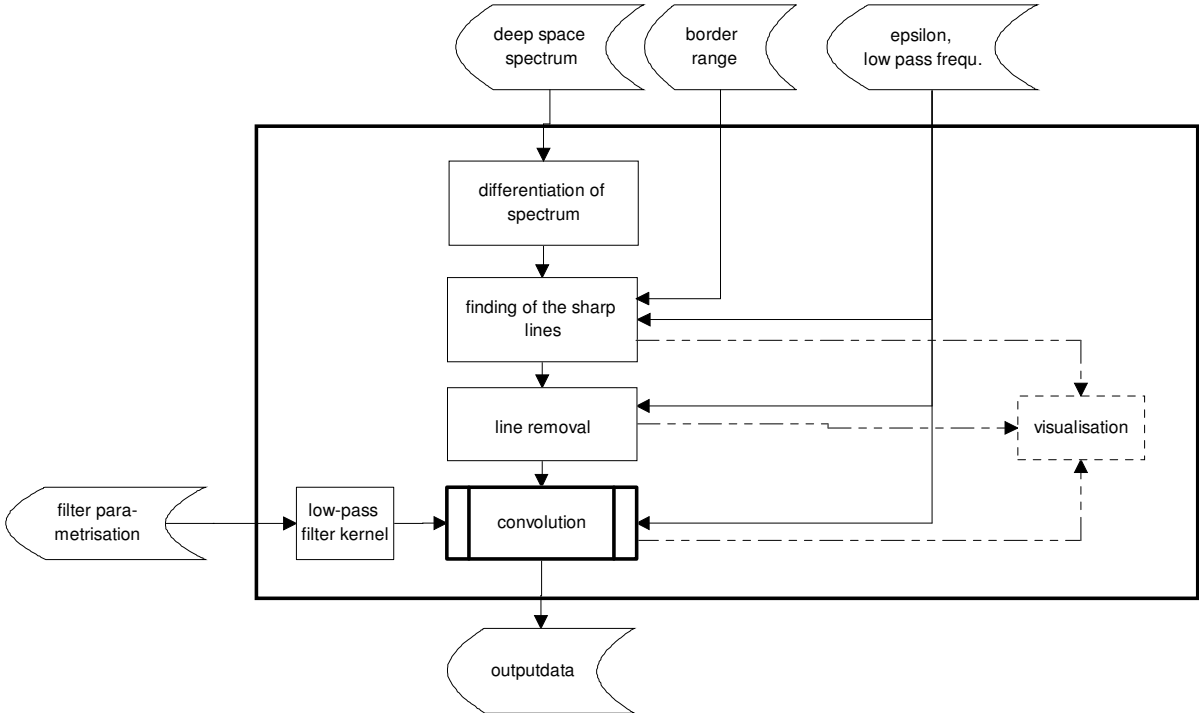
$$S' = \frac{\partial S}{\partial \sigma}, \quad S'' = \frac{\partial^2 S}{\partial \sigma^2}$$
$$S^d = \sqrt{\left(\frac{S'}{\max(|S'|)}\right)^2 + \left(\frac{S''}{\max(|S''|)}\right)^2}$$

Since no absorption lines are expected in the atmospheric spectra the sign of the derivatives needs not to be regarded.

Task two is the replacement of these lines selected for removal. Due to the small width of the selected lines, the baseline intensity can be assumed to be linear over the width of the line to remove. This leads to a linear replacement of the selected line. This process will be called "shaving" of spectra.

To reduce the noise in the 'shaved' spectrum and to smooth the edges of the replacement interval, the 'shaved' spectrum is low-pass filtered with an edge-frequency guaranteeing the preservation of the spectral baseline. In case of channeling the low-pass filter is adjusted to the frequency of the channelling effect corresponding to the displacement of the channels from ZOPD in the interferogram.

Process flowchart



## Definitions of variables

Variable	Description	I/O	Type	Remarks
order	order of the kernel	l	i	default value := 100
gibb	reduction of the Gibb's phenomena	l	r	expressed in dB
$k_m$	kernel function	t	r	
$f_h$	higher frequency of the filter in fractions of the Nyquist frequency	l	r	
$\alpha$	Bessel coefficient	t	r	
$S_m$	initial spectrum	l	r	
$S'_m$	differential spectrum	t	r	
$S_m^d$	quasi normalised spectrum	t	r	
$I_m$	Indicator vector	t	r	
m	index	t	i	
$\epsilon$	Indicator limit	l	r	default value := 0.9
r	extended area in which the spectrum is interpolated	l	i	default value := 3*resolution of the spectrum
v	index-vector of high derivative values	t	i	Initial value: $v := \{\}$

## Algorithm

### Differentiation of spectra

An indicator value is build up of the first and second derivative of the spectrum to be shaved. Both derivatives are normalized to their maximum values and their absolute values are taken to perform a geometric mean value, which is again normalized.

$$S'_m = \frac{S_{m+1} - S_{m-1}}{\sigma_{m+1} - \sigma_{m-1}}$$

$$S''_m = \frac{S'_{m+1} - S'_{m-1}}{\sigma_{m+1} - \sigma_{m-1}}$$

$$S_m^d = \sqrt{\left(\frac{S'_m}{\max(|S'_m|)}\right)^2 + \left(\frac{S''_m}{\max(|S''_m|)}\right)^2}$$

$$I_m = \frac{S_m^d}{\max(S_m^d)}$$

### Detection of sharp lines

The vector  $v$  is populated with the index of those points whose indicator  $I_m$  is higher than  $\varepsilon$ . Each detected interval is extended by  $r$  points to the left and the right to cover also the 'feet' of the sharp lines in the interval.

$$\text{if } I_m > \varepsilon \text{ then } v = \{v, m - r \dots m + r\}$$

### Removal of lines

All spectral points of the vector  $v$  are linearly interpolated. As anchor points of the linear interpolation those points are used which are most adjacent to the point to be interpolated and are not members of the vector  $v$ .

### Low pass filter kernel

The digital filtering is performed by convolution of the spectrum with a kernel function representing the low-pass filter.

The kernel function returns the coefficients of a non-recursive, digital filter for evenly spaced data points. The kernel coefficients are Kaiser weighted. The intensity of the Gibbs phenomenon wiggles is defined in -db; a value of 50 or more should be appropriate. Frequencies are expressed in terms of the Nyquist frequency,  $1/d\sigma/2$ , where  $d\sigma$  is the interval between data samples. The resulting vector of coefficients has  $(2 \cdot \text{order} + 1)$  elements.

$$\alpha = \begin{cases} 0 & \text{for } \text{gibb} \leq 21 \\ 0.5842(\text{gibb} - 21.)^{0.4} + 0.07886(\text{gibb} - 21.) & \text{for } 21 < \text{gibb} < 50 \\ 0.1102(\text{gibb} - 8.7) & \text{for } \text{gibb} \geq 50 \end{cases}$$

$$k_{m+\text{order}} = \frac{\sin(i\pi f_h)}{i\pi} \frac{\mathbf{I}\left(\alpha \sqrt{1 - \left(\frac{m}{\text{order}}\right)^2}, 0\right)}{\mathbf{I}(\alpha, 0)} \quad m = [1..\text{order}]$$

$$k_{\text{order}} = f_h$$

$$k_{m-1} = k_{2\text{order}-m+1}$$

with  $\mathbf{I}(\alpha, x)$ : Besselfunction

## 9. References

[DPAD1995]

**MIPAS Data Processing and Algorithm Development Subgroup**

*Report*

European space agency, December 1994

[Carlotti 1998]

**Carlotti,M., Höpfner,M., Raspollini,P., Ridolfi,M., Carli,B.**

*Technical note for ESA on: High level algorithm definition and physical and mathematical optimisations*

Document: TN-IROE-RSA9601, European space agency, October 1998

[Ende1993]

**Endemann,M., Lange.G., Fladt,B.**

*Michelson Interferometer for Passive Atmospheric Sounding,*

SPIE Proceedings, Vol. 1034, 1993

[Fill1964]

**Filler,A.S.**

*Apodization and Interpolation in Fourier-Transform Spectroscopy,*

Journ. of the Optical Society of America; Vol. 54; No. 6, June 1964

[Form1966]

**Forman,M.L., Steel,W.H., Vanasse,G.**

*Correction of Asymmetric Interferograms Obtained in Fourier Spectroscopy*

Journ. of the Optical Society of America; Vol. 56; No. 1, Page 59-63, January 1966

[Frie1999-1]

**Friedl-Vallon, F., et al.,**

*The balloonborne Michelson Interferometer for Passive Atmospheric Sounding (MIPAS-B2) - Instrument and Results,*

Proc. SPIE Vol. 3756, p.9-16, 1999.

[Frie1999-2]

**Friedl-Vallon,F., Maucher, G., Trieschmann, O., Oelhaf, H.**

*Instrument Characterisation of MIPAS-B2*

Revision 1, 22.12.1999

ESA-Contract No. 12078/96/NL/GS

[LEVEL1B]

**ESA-Contract**

*DPM/PDL*

PO-RP-BOM-GS-0003

**ESA-Contract**

*IODD*

PO-TN-BOM-GS-0010

[Mauc1999]

**Maucher, G.,**

*Das Sternreferenzsystem von MIPAS-B2: Sichtlinien-Bestimmung für ein ballongetragenes Spektrometer zur Fernerkundung atmosphärischer Spurengase,*  
Ph.D. Thesis for physics at the “Institut für Meteorologie und Klimaforschung” of the University of Karlsruhe and “Forschungszentrum Karlsruhe”, Rep. FZKA 6227, Forschungszentrum Karlsruhe GmbH, Karlsruhe, Germany, 1999

[Nort1976]

**Norton, R.H., Beer, R.**

*New Apodization functions for Fourier Spectroscopy*

Journ. of the Optical Society of America; Vol. 66; No. 3, June 1976

**Norton, R.H., Beer, R.**

*Erratum to New Apodization functions for Fourier Spectroscopy*

Journ. of the Optical Society of America; Vol. 67; No. 3, P. 419  
March 1977

[Pres1986]

**Press, W.H., Flannery, B.P., Teukolsky, S.A., Vetterling, W.T.**

*Numerical Recipes*

Cambridge University Press, 1986

[Reve1988]

**Revercomb, H.E., et al.**

*Radiometric calibration of IR Fourier transform spectrometers: solution to a problem with the High-Resolution Interferometer Sounder*

Applied Optics, Vol. 27, No. 15, 3210-3218

[Seef1995]

**Seefeldner, M, Keim, C., M.Maucher, G.**

*The pointing and the star reference system of the MIPAS-B2 gondola*

Proc. 12<sup>th</sup> ESA symposium on rocket & balloon programs and related research, May 1995, Lillehammer, Norway

[Still1998]

**G.P.Stiller et al., M. Höpfner et al., M. Kuntz et al.,**

*The Karlsruhe optimized and precise radiative transfer algorithm.*

Part I-III, Jinxue Wang, Beiying Wu, Toshihiro Ogawa, Zheng-hua Guan, Editors, Proceedings of SPIE Vol. 3501, 257-268, 186-195, and 247-256 (1998)

[Trie1997-1]

**Trieschmann,O.**

*The need of a precise phase-correction for radiometric calibration*

Proc. 7<sup>th</sup> int. Workshop on Atmospheric Science from Space using FTS, DLR Oberpfaffenhofen, Germany; May 1997

[Trie1997-2]

**Trieschmann,O., Kapetanios,E., Lorenz,H.P.**

*A Database Design and Implementation for Scientific Data Related to the MIPAS-Balloon-Spectrometer*

In: Lautenschlager,M. and Reinke,M. (ed.): Climate and Environmental Database Systems, Kluwer Academic Publishers, Boston, 1997

[Trie2000]

**Trieschmann,O.,**

*Phasenkorrektur und Radiometrie gekühlter Fourierspektrometer: Charakterisierung des Instrumentes MIPAS-B2*

Ph.D. Thesis for physics at the "Institut für Meteorologie und Klimaforschung" of the University of Karlsruhe and "Forschungszentrum Karlsruhe", Rep. FZKA 6411, Forschungszentrum Karlsruhe GmbH, Karlsruhe, Germany, 2000

[Walr1984]

**Walraven,R.**

*Digital Filters*

Proceedings of the Digital Equipment User's Society, Fall, 1984.

Department of Applied Science, University of California, Davis, CA 95616.

[Wedd1993]

**Weddigen,Ch., Blom,C.E., Höpfner,M.**

*Phase correction for the emission sounder MIPAS-FT*

Applied Optics, 32, 4586-4589

## 10. Appendix

### 10.1. Abbreviation and Notation

#### Abbreviations:

AHRS	Attitude and Heading Reference System
DPAD	Data Processing and Algorithm Development subgroup
FTS	Fourier Transform Spectrometer
IFG	Interferogram
LOS	Line Of Sight
OPD	Optical Path Difference
POPD	Peak position of the IFG
SAG	Scientific Advisory Group for the MIPAS/ENVISAT instrument
ZOPD	Zero Optical Path Difference

#### Physical and mathematical and programming expressions:

$A(x)$	apodisation function
$FFT^+(\cdot)$	Fast Fourier Transform
$FFT^-(\cdot)$	inverse Fast Fourier Transform
$I(x)$	radiance of the interferogram
$Im(\cdot)$	imaginary part of a complex quantity
<code>greg2julian()</code>	conversion of time and date in standard format to julian time
<code>julian2greg()</code>	conversion of julian time to time and date in standard format
<code>indexof()</code>	index of the specific element of a vector
<code>max()</code>	maximum value of a function or vector
<code>min()</code>	minimum value of a function or vector
$Re(\cdot)$	real part of a complex quantity
$RECT(\cdot)$	rectangular function
$S(\sigma)$	spectral radiance
$x$	optical path difference
$\sigma$	wavenumber

#### Phase definitions:

instrumental phase	phase introduced by optical components
linear phase	phase error due to shifts of the digitalisation
classical phase determination	phase determination method by [Form1996]
differential phase determination	phase determination method by [Wedd1993]
statistical phase determination	phase determination method by [Trie1997-1]

## 10.2. List of wavenumbers of critical radiometric calibration

Lines are indicated which introduce due to their behavior in the blackbody spectra an error in the calibrated spectra greater than  $3\sigma$  of NESR.

### 10.2.1. Channel 1

Selected CO<sub>2</sub>-Lines which should not be used for p,T-retrieval.

	Wavenumber	Intensity	E''
1	685.554871	1.57E-19	197.4166
2	685.969627	2.27E-21	865.32
3	687.110635	2.11E-21	882.9715
4	687.154843	1.35E-19	234.0833
5	688.757796	1.13E-19	273.868
6	688.77566	1.79E-21	921.2382
7	690.363693	9.28E-20	316.7698
8	690.448474	1.47E-21	962.6257
9	691.972498	7.41E-20	362.7882
10	693.584173	5.78E-20	411.9225
11	695.198683	4.40E-20	464.1717
12	696.815987	3.28E-20	519.535
13	698.436046	2.38E-20	578.0116
14	700.058822	1.70E-20	639.6004
15	701.684272	1.18E-20	704.3005
16	703.312356	8.03E-21	772.1107
17	704.943031	5.34E-21	843.0301
18	706.576255	3.48E-21	917.0573
19	708.211983	2.22E-21	994.1913
20	720.638622	2.50E-21	728.4124
21	720.687389	2.36E-21	710.4163
22	720.727743	2.09E-21	695.5496
23	720.759644	1.73E-21	683.8124
24	720.783063	1.26E-21	675.205

## 10.2.2. Channel 2

Selected H<sub>2</sub>O -Lines which should not be used for trace-gas-retrieval.

	wavenumber	intensity	E"
1	1387.5229	2.04E-20	742.0764
2	1394.4745	3.19E-20	610.3413
3	1399.2042	3.19E-20	508.8122
4	1419.508	7.23E-20	488.1078
5	1436.8182	8.53E-20	382.5169
6	1456.8871	1.63E-19	285.4186
7	1458.267	5.45E-20	285.2194
8	1464.9051	9.33E-20	212.1564
9	1472.0512	9.79E-20	300.3623
10	1473.5142	7.56E-20	447.2524
11	1487.3485	5.24E-20	206.3014
12	1496.2489	1.31E-19	325.3479
13	1498.8032	6.49E-20	136.1639

### 10.2.3. Channel 3

Selected H<sub>2</sub>O -Lines which should not be used for trace-gas-retrieval.

	Wavenumber	Intensity	E''
1	1558.5309	2.68E-19	173.3658
2	1560.2572	2.35E-19	212.1564
3	1569.7887	1.27E-19	95.1759
4	1576.1855	3.66E-19	42.3717
5	1616.7115	3.37E-19	23.7944
6	1623.5592	1.12E-19	70.0908
7	1627.8275	5.84E-20	37.1371
8	1634.9671	8.83E-20	0
9	1635.6519	2.18E-19	136.7617
10	1637.5119	3.95E-20	134.9016
11	1645.9693	1.84E-19	173.3658
12	1647.4041	4.62E-20	275.4971
13	1648.3105	4.99E-20	95.1759
14	1652.4003	3.03E-19	79.4964
15	1653.2671	3.47E-19	23.7944
16	1653.417	3.61E-20	222.0528
17	1654.5112	7.09E-20	399.4576
18	1662.8093	1.06E-19	79.4964
19	1669.3929	1.27E-19	70.0908
20	1671.5091	3.50E-20	142.2785
21	1675.1728	1.10E-19	142.2785
22	1675.5152	4.64E-20	325.3479
23	1683.178	7.07E-20	224.8384
24	1684.8352	3.58E-19	136.7617
25	1695.4594	4.97E-20	212.1564
26	1695.9282	2.75E-19	224.8384
27	1699.9339	2.47E-19	42.3717
28	1700.5008	6.67E-20	300.3623
29	1700.7763	9.40E-20	222.0528
30	1704.4534	4.64E-20	300.3623
31	1706.3493	7.00E-20	37.1371
32	1715.1551	6.18E-20	326.6255
33	1717.4055	1.86E-19	325.3479
34	1718.6117	6.65E-20	95.1759
35	1733.3906	1.05E-19	447.2524
36	1734.6506	1.48E-19	173.3658
37	1739.8388	1.18E-19	79.4964

## **10.3.Data exchange for MIPAS-B balloon data between IMK and IROE/Univ. of Bologna**

Based on the memorandum prepared by H. Oelhaf, M. Höpfner, O. Trieschmann (IMK), B. Dinelli (University of Bologna), and M. Ridolfi (IROE-CNR) on 25.9.1998 the calibrated spectra and related housekeeping data will be distributed to the users with the following updated format:

### **10.3.1. Purpose**

Referring to WP 6000 of contract 11717/95/NL/CN this memorandum defines the technical interface for the exchange of MIPAS-B balloon data between IMK and IROE/University of Bologna.

### **10.3.2. Abbreviations**

AILS	apodised instrumental line shape
c	character
FOV	field-of-view
i	integer
MPD	maximum optical path difference
r	real

### **10.3.3. Definitions and general information**

#### Scan/Sweep/nominal elevation angle

A scan is a limb scanning sequence including spectral measurements at different nominal elevation angles. At each elevation angle several sweeps (spectral measurements) are performed. Therefore, in contrast to MIPAS/ENVISAT more than one sweep can belong to the same nominal elevation angle.

#### File types

All files are in ASCII format except the calibrated spectra for ESA-Contract No. 12078/96/NL/GS which are stored in the scientific interchange format HDF.

#### Comment lines of files in ASCII-format

The first character of a comment record is a #. All other records contain data.

### **10.3.4. File formats**

Any line of comment precedes with a "#".

### 10.3.4.1. Channel descriptive data sets (ESA-Contract No. 11717/95/NL/CN and ESA-Contract No. 12078/96/NL/GS)

File name

MIP-B-Vx-Cy

where x is the data version and y the channel number.

Type

ASCII

Field name	Format	Units	Comments
Data version	i		
Channel	i		
Boundary of vertical FOV distribution	r	degree	The FOV is assumed to extend from -boundary, to +boundary
FOV coefficients	r(9)		The FOV is parameterised as a polynomial of 8th order. Negative FOV angles refer to higher elevation
MPD of the measurement	r	cm	
Ratio of zerofilling	r		
AILS parameters	r(7x3)		
Elevation- a posteriori knowledge	r	arcmin	3 $\sigma$ standard deviation
Observer altitude- a posteriori knowledge	r	km	3 $\sigma$ standard deviation
Number of nominal elevations	i		
<i><u>Begin nominal elevation 1 ... number of nominal elevations</u></i>			
Nominal elevation	r	degree	
Filename of variance spectrum	c		
Number of sweeps	i		
<i><u>Begin sweep 1 ... number of sweeps</u></i>			
Filename of measured spectrum	c		
<i><u>End sweep 1 ... number of sweeps</u></i>			
<i><u>End nominal elevation 1 ... number of nominal elevations</u></i>			

### 10.3.4.2. Spectral data sets (ESA-Contract No. 11717/95/NL/CN)

File name

MIP-B-Vx-Cy-Ez-Sn.ascii

where x is the data version, y the channel number, z the nominal elevation angle, and n the number of the spectrum (as derived in subsection 7.5).

n = 0 refers to the standard deviation spectrum (as derived in subsection 7.5.3).

Type

ASCII

Field name	Format	Units	Comments
Data version	i		
Channel	i		
Nominal elevation angle	r	degree	
Acquisition date	c		given as 'dd.mm.yy'
Acquisition time	c		given as 'hh:mm:ss'
Latitude of observer	r	degree	
Longitude of observer	r	degree	from -180 to +180 with positive eastern longitudes
Altitude of observer	r	km	
Elevation angle	r	degree	negative angles looking downward
Azimuth angle	r	degree	from 0 to 360: N->E->S->W->N
Latitude of tangent point	r	degree	includes refraction using initial guess p-T profile
First wavenumber	r	cm <sup>-1</sup>	
Wavenumber grid interval	r	cm <sup>-1</sup>	
Number of grid points	i		
<i><u>Begin grid point 1 ... number of grid points</u></i>			
wavenumber, intensity	r(2)	cm <sup>-1</sup> , W/cm <sup>2</sup> Srcm <sup>-1</sup>	
<i><u>End grid point 1 ... number of grid points</u></i>			

### 10.3.4.3. Spectral data sets (ESA-Contract No. 12078/96/NL/GS)

#### File name

MIP-B-Vx-Cy-Ez-Sn.hdf

where x is the data version, y the channel number, z the nominal elevation angle, and n the number of the spectrum (as derived in subsection 7.5).

n = 0 refers to the standard deviation spectrum (as derived in subsection 7.5.3).

#### Type

HDF

The HDF data format is used for exchange of MIPAS-B2 data between ESA and the contractor. Further information about HDF can be found on the World Wide Web [HDF1999].

The information content is identically to the one described in subsection 10.3.4.2. The following source code is written in IDL, which condenses the data to the HDF-files:

```
-----  
; Procedure to construct the HDF files using IDL  
-----  
  
pro esa_hdf,filename,latitude,longitude,altitude,realelev,azimuth,lattangent  
  
    arr = read_XYfile(strmid(filename,0,21)+'.bin',time=time)  
    filename = strmid(filename,0,21)+'.hdf'  
    sd_id = HDF_SD_START(filename, /CREATE)  
    HDF_DFAN_ADDFDS, filename, 'Spectrum of the MIPAS-B2 Flight from Aire sur  
1'Adour,1998 (c) IMK/FZK'  
    HDF_SD_ATTRSET, sd_id, 'Filename', filename  
    HDF_SD_ATTRSET, sd_id, 'Data version', strmid(filename,7,1)  
    HDF_SD_ATTRSET, sd_id, 'Channel', fix(strmid(filename,10,1))  
    HDF_SD_ATTRSET, sd_id, 'Nominal elevation angle', loat(strmid(filename,13,5))  
    HDF_SD_ATTRSET, sd_id, 'Acquisition date', strmid(time,5,8)  
    HDF_SD_ATTRSET, sd_id, 'Acquisition time', strmid(time,14,8)  
    HDF_SD_ATTRSET, sd_id, 'Latitude of observer', latitude  
    HDF_SD_ATTRSET, sd_id, 'Longitude of observer', longitude  
    HDF_SD_ATTRSET, sd_id, 'Altitude of observer', altitude  
    HDF_SD_ATTRSET, sd_id, 'Elevation angle', realelev  
    HDF_SD_ATTRSET, sd_id, 'Azimuth angle', azimuth  
    HDF_SD_ATTRSET, sd_id, 'Latitude of tangent point', lattangent  
    HDF_SD_ATTRSET, sd_id, 'First Wavenumber', arr[0,0]  
    HDF_SD_ATTRSET, sd_id, 'Wavenumber grid interval', 0.025d0  
    sz=size(arr)  
    HDF_SD_ATTRSET, sd_id, 'Number of grid points',sz(1)  
    if sz(0) eq 0 then return  
    sds_id = HDF_SD_CREATE(sd_id, 'Spectrum [Wavenumber,Intensity]', sz(1:sz(0)),  
/DOUBLE)  
    HDF_SD_ADDDATA, sds_id, arr ;Write the data into the dataset.  
    HDF_SD_ENDACCESS, sds_id ;End access to any SD IDs.  
    HDF_SD_END, sd_id ;When finished with the file, close it with a call to  
  
return  
  
end
```

**10.3.4.4. Pressure-temperature initial guess profile (ESA-Contract No. 11717/95/NL/CN and ESA-Contract No. 12078/96/NL/GS)**

File name

MIP-B-Vx-PT

where x is the data version.

Type

ASCII

<b>Field name</b>	<b>Format</b>	<b>Units</b>	<b>Comments</b>
Number of atmospheric levels	i		
Altitude of atmospheric levels	r(number of levels)	km	
Pressure at levels	r(number of levels)	hPa	
Temperature at levels	r(number of levels)	K	

## 10.4. HDF data format description of delivered data

The HDF data format has been agreed for exchange of MIPAS-B2 data between ESA and the contractor.

### General format used within HDF:

The Hierarchical Data Format (HDF) is a multi-object file format that facilitates the transfer of various types of data between machines and operating systems. HDF is a product of the National Center for Supercomputing Applications (NCSA). HDF is designed to be flexible, portable, self-describing and easily extensible for future enhancements or compatibility with other standard formats. The HDF library contains interfaces for storing and retrieving images and multi-dimensional scientific data.

Further information about HDF can be found on the World Wide Web. The HDF "Frequently-Asked Questions" file can be found at:

<http://hdf.ncsa.uiuc.edu:8001/HDF-FAQ.html>

The following source code is written in IDL, which supports HDF3\_3r4, and retrieves the metadata from the HDF-file giving information on the data and its formats stored within this file:

```
pro testhdf,filename,OUTFILE=outfile

; displays Raster,SD,MSDS and Vset information about filename,
; in tabular format

F4='(A,I15) '
F5='(A14," ",A8," ",A5) '
FS='(A14," ",A8," : ",A) '
FF='(A14," ",A8," : ",F) '
FD='(A14," ",A8," : ",D) '

; Check for required number of input parameters
if n_params() lt 1 then begin
  print,'usage: hdfest,filename [,OUTFILE=outfile] '
  print," ARGUMENTS : filename : string name of HDF file"
  print," KEYWORDS:"
  print," OUTFILE : filename for output information"
  print," to be written to (optional)"
  print,' OUTPUTS: the HDF metadata for this file,'
  print,' always to the display, and possibly'
  print,' to the outfile specified'
  print,"EXAMPLE: hdfinfo,'demo.hdf'"
  print,'will display the HDF metadata for this file'
  return
endif

; Check that it is HDF !
if hdf_ishdf(filename) ne 1 then begin
  message,"File "+filename+" is not an HDF file."
endif

; Open the HDF file readonly
fileid=hdf_open(filename,/read)
print," *****BEGINNING OF HDF_INFORMATION***** "
print
print," FILENAME : ",filename

; Get the number of file descriptions and read them.
numdesc=hdf_number(fileid,tag=101)>0
```

```

print, ''
if numdesc eq 1 then begin
    hdf_dfan_getfds, filename, desc, /first
    print, " FILE DESCRIPTION      :"
    print, '    '+string(desc)
endif

;      Get the number of SDSs in the file
numndg=hdf_number(fileid,tag=721)>0
numsd=hdf_number(fileid,tag=701)>0
numsd=hdf_number(fileid,tag=702)>0
hdf_dfsd_getinfo, filename, NSDS=numsd
print, ''
print, ' # OF SDS                  : ', numsd, FORMAT=F4

sd_id=HDF_SD_START(filename, /read)
HDF_SD_FILEINFO, sd_id, nmfsds, nglobatts
;      Get the number of file descriptions and read them.
print, ''
print, ' # OF GLOBAL ATTRIBUTES : ', nglobatts, FORMAT=F4
if nglobatts gt 0 then begin
print, " -----"
print, 'Name', 'Type', 'Value', FORMAT=F5
print
for i=0, nglobatts-1 do begin
    HDF_SD_ATTRINFO, sd_id, i, name=n, type=t, data=d
;      if (c ne 1) then print, strtrim(n), t, c, FORMAT=F4 else $
    if (t eq 'STRING' ) then print, strtrim(n), t, d(0,0), FORMAT=FS else $
    if (t eq 'FLOAT' ) then print, strtrim(n), t, d(0,0), FORMAT=FF else $
    if (t eq 'DOUBLE' ) then print, strtrim(n), t, d(0,0), FORMAT=FD else $
    print, strtrim(n), t, d(0,0), FORMAT=FI
endfor
print, " -----"
endif

;      Get the number of MFSDs in the file
print, ''
print, " # of MFSD                  : ", nmfsds, FORMAT=F4
if nmfsds gt 0 then begin
print, " -----"
FSS='(A15, " ", A4, " ", A8, " ", A5, " ", A5)'
print, 'Name', 'Rank', 'Type', 'Size', 'Value', Format=FSS
print, ''
FSD='(A15, " ", I4, " ", A8, " ", I5, " ", A)'
for i=0, nmfsds-1 do begin
    sds_id=HDF_SD_SELECT(sd_id, i)
    HDF_SD_GETINFO, sds_id, name=n, ndims=r, type=t, natts=nats, dims=dims
    HDF_SD_GETDATA, sds_id, data
    if dims gt 1 then begin
        print, n, r, t, dims, FORMAT=FSD
        plot, data
    endif else print, n, r, t, dims, string(data), FORMAT=FSD

    HDF_SD_ENDACCESS, sds_id
endfor
print, " -----"
endif

HDF_SD_END, sd_id
print
print, " *****END OF HDF_INFORMATION***** "
hdf_close, fileid

end

```

## 10.5. ILS calculation from Bessel coefficients

As described in subsection 6.5.1, the ILS can be directly obtained by adding spherical Bessel functions which are weighted by a set of coefficients  $c_i$ . These Bessel coefficients are given as a polynomial of second order over the wavenumber. The printed IDL-program gives an example on how to calculate the ILS from a set of Bessel functions without using a mathematical library for Bessel functions.

```
=====
; Procedure to calculate the ILS/AALS from given Bessel coefficients.
;
;       (c) Olaf Trieschmann, 1998
;       Forschungszentrum Karlsruhe/
;       Institut für Meteorologie und Klimaforschung
;
;-----
;
; VARIABLES
;
; sigma0 :      wavenumber for which the AALS is to be calculated
;
; KEYWORDS
;
; nhalf :      number of points on each side of the center with a
;              a sampling interval of 0.025cm-1
; d_grid :      gridspacing
; d_resol :     the nominal resolution, respectively the optical path
; Ci :         Coefficients of the Modulation function; if this keyword is set
;              then any value to channel and sigma0 are obsolete
;
;-----
; Revisions:
; 15.2.2000:    Appending and reorganizing of the variables and keywords
;              nhalf,channel,d_grid,d_resol
;=====

function bessel_ifg, sigma0, nhalf=nhalf, d_grid=d_grid, d_resol=d_resol, Ci=Ci

if not(keyword_set(nhalf)) then nhalf = 10

; the nominal resolution, respectively the optical path
if not(keyword_set(d_resol)) then d_resol = 0.0345

; gridspacing
if not(keyword_set(d_grid)) then d_grid = 0.025

; the AALS coefficients (Channel 1)
ai0 = [-1.313E-08, 6.343E-08, -2.610E-07, 8.264E-07, -1.344E-06, 1.172E-06, -8.853E-07, 4.417E-07]
ai1 = [1.070E-05, -8.484E-05, 2.686E-04, -1.102E-03, 1.778E-03, -1.525E-03, 1.213E-03, -5.594E-04]
ai2 = [4.014E-02, +3.115E-02, +4.446E-01, 4.020E-01, -2.177E-01, 5.287E-01, -4.119E-01, 1.830E-01]

if not(keyword_set(Ci)) then begin
; calculation of the coefficients vs. wavenumber
ci = dblarr(n_elements(ai0))
for i = 0, (n_elements(ai0)-1) do begin
    ci[i] = ai0[i]*sigma0^2 + ai1[i]*sigma0 + ai2[i]
endfor
endif

; creation of the abscissa and ordinate vector with 2*nhalf
; elements set to zero
ils = dblarr(2*nhalf+1.0)
sigma = dblarr(2*nhalf+1.0)
; creation of the abscissa working vector of nhalf points.
; The value of the elements are set to their index
sigmatmp = (dindgen(nhalf)+1.0)*d_grid/d_resol*!DPI

zero = dblarr(nhalf)
fm = dblarr(nhalf,9)
gm = dblarr(nhalf,9)
;n=1/2
fm[* ,0] = zero+1.0
gm[* ,0] = zero
;n=3/2
fm[* ,1] = 1.0/sigmatmp
gm[* ,1] = zero+1.0
;n=5/2
fm[* ,2] = 3.0/sigmatmp^2-1.0
```

```

gm[* ,2] = 3.0/sigmatmp
;n=7/2
fm[* ,3] = 15.0/sigmatmp^3-6.0/sigmatmp
gm[* ,3] = 15.0/sigmatmp^2-1
;n=9/2
fm[* ,4] = 105.0/sigmatmp^4-45.0/sigmatmp^2+1.0
gm[* ,4] = 105.0/sigmatmp^3-10.0/sigmatmp
;n=11/2
fm[* ,5] = (945.0/sigmatmp^3-420.0/sigmatmp^1)/sigmatmp^2+15.0/sigmatmp
gm[* ,5] = (945.0/sigmatmp^2-105.0)/sigmatmp^2+1.0
;n=13/2
fm[* ,6] = (10395.0/sigmatmp^3-4725.0/sigmatmp^1)/sigmatmp^3+210.0/sigmatmp^2-1.0
gm[* ,6] = (10395.0/sigmatmp^3-1260.0/sigmatmp^1)/sigmatmp^2+21.0/sigmatmp
;n=15/2
fm[* ,7] = ((135135.0/sigmatmp^3-62370.0/sigmatmp^1)/sigmatmp^2+3150.0/sigmatmp^1)/sigmatmp^2-28.0/sigmatmp
gm[* ,7] = (135135.0/sigmatmp^4-17325.0/sigmatmp^2)/sigmatmp^2+378.0/sigmatmp^2-1.0
;n=17/2
fm[* ,8] = (2027025.0/sigmatmp^4-945945.0/sigmatmp^2)/sigmatmp^4+51975.0/sigmatmp^4-630.0/sigmatmp^2+1.0
gm[* ,8] = (2027025.0/sigmatmp^4-270270.0/sigmatmp^2)/sigmatmp^3+6930.0/sigmatmp^3-36.0/sigmatmp

; the tabulated Gammafunction: [GAMMA(1)..GAMMA(8)]
gamm = [+1.000E+00,+1.000E+00,+2.000E+00,+6.000E+00,+2.400E+01,+1.200E+2,    $
        +7.20E+2,+5.040E+3,+4.0320E+4,+3.62880E+5]
norm = [1.0, 2.0/3.0, 8.0/15.0, 48.0/105.0, 384.0/945.0, 3840.0/10395.0, 46080.0/135135.0, $
        645120.0/2027025d0, 10321920d0/34459425d0]

for i = ((n_elements(ci)-1) < 8),0, -1 do begin
    a = gamm[i] * 2d0^(-1) * (fm[* ,i]*sin(sigmatmp) - gm[* ,i]*cos(sigmatmp))
    a = ci[i] * a
    ils[nhalf+1:2*nhalf] = 2d0*(ils[nhalf+1:2*nhalf] + a)/sigmatmp
endfor
ils[0:nhalf-1] = reverse(ils[nhalf+1:2*nhalf])
ils[nhalf] = total(norm[0:(n_elements(ci)-1)]*ci)

; scaling of the wavenumber axis to the nominal resolution
sigma[nhalf+1:2*nhalf] = sigmatmp*d_resol!/DPI
sigma[0:nhalf-1] = -reverse(sigma[nhalf+1:2*nhalf])

for i = 0,5 do begin
    print,sigma[nhalf+i],ils[nhalf+i]
endfor

return, [[sigma],[ils]]

end

```